Lake volume and potential hazards of moraine-dammed glacial lakes in temperate glaciation regions—A case study of Bienong Co

Hongyu Duan[1], Xiaojun Yao[1], Yuan Zhang[1], Huian Jin[2], Qi Wang[3], Zhishui Du[3], Jiayu Hu[1], Bin Wang[4], and Qianxun Wang[5]

[1] College of Geography and Environment Science, Northwest Normal University, LanZhou, 730070, China
[2] Gansu Forestry Polytechnic, Tianshui, 741020, China
[3] Northwest Engineering Corporation Limited, Power China, Xi'an 710065, China
[4] Xinjiang Transport Planning Survey and Design Institute Company Limited, Urumqi 830006, China
[5] Capital Urban Planning and Design Consulting Development Company Limited, Beijing 100038, China

Correspondence to: Xiaojun Yao (xj_yao@nwnu.edu.cn)

Abstract. The existence of glacial lakes in the Southeastern Tibetan Plateau (SETP) is a potential hazard to downstream regions, as the outburst of ~~some~~ lakes has the potential to result in disastrous glacial lake outburst flood (GLOF) ~~events of high-magnitude~~. In the present study, we conducted a comprehensive investigation for Bienong Co, an ~~end~~ moraine-dammed glacial lake in SETP. First, the lake basin morphology was ~~simulated~~ and the lake volume was estimated, showing that the maximum lake depth is ~181 m and the lake volume is ~102.3×10^6 m^3. Then, we assumed that the ice avalanche (Scenarios A1, A2, and A3) and the lateral moraine landslide (Scenarios B1, B2, and B3 and C1, C2, and C3) induced GLOFs process chain of Bienong Co. The volume of nine trigger scenarios was calculated using the RAMMS model, and the displacement wave generation and propagation in the lake, overtopping flow and erosion on the moraine dam, and subsequent downstream flooding were simulated by the BASEMENT model. The results ~~demonstrate~~ that the ice avalanche scenarios ~~produce~~ the largest amount of material into the lake, resulting in displacement wave ~~amplitudes~~ of up to 25.2 m (Scenario A3) ~~near the moraine dam~~. Smaller ~~volumes of~~ landslides entering the lake ~~only~~ result in smaller displacement waves ~~in the lake, such as that Scenario C1 has a wave amplitude below 1 m near the moraine dam~~. Scenarios A1, A2, and A3 result in released water from the lake of 24.1 × 10^6 m^3, 25.3 × 10^6 m^3, and 26.4 × 10^6 m^3~~,~~ ~~and~~ peak discharges at the moraine dam of 4,996 m^3/s, 7,817 m^3/s, and 13,078 m^3/s, respectively. These high discharges cause scour erosion of the moraine dams, resulting in breach widths of 295~~.0~~ m, 339~~.4~~ m, and 368~~.5~~ m, and breach depths of ~~19.0 m, 19.1 m, 19.3~~ m~~, respectively~~. ~~However, in~~ landslide scenarios, only the overtopping flow generated by Scenarios B3 and C3 caused ~~moderate~~ erosion of the moraine dam, with breach depths of 6.5 m and 7.9 m, and breach widths of 153 m and 169 m, respectively. GLOFs generated by Scenario A1, A2, and A3 ~~can~~ all flow through 18 settlements downstream, ~~and will threaten~~ more than half of the settlements. Both Scenarios B3 and C3 produced ~~floods~~ that flow through eight downstream settlements within 20 h and had a relatively small impact on them. Comparisons show that Bienong Co is the relative deepest glacial lake known on the Tibetan Plateau, and this study could provide new insight about moraine-dammed glacial lakes in the SETP and a valuable reference for GLOFs disaster prevention for local governments.

1 Introduction

Due to global warming, accelerated retreat and thinning of glaciers has occurred in most regions compared to the last century (Zemp et al., 2019), resulting in a rapid increase in the number, area, and volume of glacial lakes worldwide (Shugar et al., 2020; Wang et al., 2020). Glacier meltwater can be confined and stored in certain depressions dammed by moraine, ice, or bedrock (Vilímek et al., 2013). Once the dam is damaged, the water can be suddenly and catastrophically released to form glacial lake outburst floods (GLOFs), which may cause severe social and geomorphic impacts several dozens of kilometers and more downstream (Lliboutry, 1977; Richardson and Reynolds, 2000; Osti and Egashira, 2009; Carrivick and Tweed,

2016; Cook et al., 2018; Harrison et al., 2018; Zheng et al., 2021). Moraine-dammed glacial lakes are of particular concern due to their large volume (Fujita et al., 2013; Veh et al., 2019), weak dam composition, and exposure to various triggers, such as ice and/or rock avalanches, heavy precipitation, and intense glacier melting (Emmer and Cochachin, 2013; Nie et al., 2018), which are the most common sources of GLOFs (Watanbe and Rothacher, 1996; Westoby et al., 2014). The Himalayas and the Southeastern Tibetan Plateau (SETP) are regions of frequent occurrence of GLOFs caused by moraine-dammed glacial lakes (Wang, 2016). Research shows that the Himalayas, especially the southern region, are likely to experience more GLOFs in the coming decades (Veh et al., 2019).

The SETP is a broad mountainous area covering the central and eastern Nyainqêntanglha Ranges, eastern Himalayas and western Hengduan Mountains, and has highly complicated terrains (Ke et al., 2014). Controlled by warm and humid Indian monsoons, a large number of temperate glaciers have developed here (Yang et al., 2008), featured as adequate recharge, strong ablation, low snowline distribution, high temperature, fast movement, and strong geological, as well as geomorphological, effect (Li et al., 1986; Qin et al., 2012; Liu et al., 2014), which have been observed with markedly negative mass balances during the past decades (Kääb et al., 2012; Neckel et al., 2014; Kääb et al., 2015; Brun et al., 2017; Dehecq et al., 2019). Therefore, the combination of active glacial processes and heavy rainfall during the monsoon season makes the region prone to glacier-related natural hazards (Wang et al., 2012b). Studies of glacial lakes in the SETP have mainly focused on regional-scale assessment of glacial lake changes (Wang et al., 2011a; Song et al., 2016; Wang et al., 2017; Zhang et al., 2020; Zhang et al., 2021), identification of potentially dangerous glacial lakes (Wang et al., 2011a; Liu et al., 2019; Duan et al., 2020; Qi et al., 2020), site-specific analysis of formation mechanisms, development trends, risk evolution and management measures of GLOFs (Cui et al., 2003; Cheng et al., 2008, 2009; Sun et al., 2014; Liu et al., 2021; Wang et al., 2021), and exploration of geological features of a single glacial lake (Yuan et al., 2012; Liu et al., 2015; Huang et al., 2016). Fewer studies have applied hydrodynamic models to simulate GLOFs in the SETP. Wang et al. (2011b) evaluated the applicability of ASTER GDEM (the Global Digital Elevation Model) and SRTM DEM in the simulation of GLOF processes based on the HEC-RAS hydrodynamic model (Brunner, 2002). Zheng et al. (2021) analyzed and reconstructed a GLOF process chain of Jinwu Co using published empirical relationships and the GIS-based r.avaflow simulation tool (Mergili et al., 2017; Pudasaini and Mergili, 2019; Mergili and Pudasaini, 2020).

As a key factor related to the peak discharge and outburst volume of a GLOF event (Evans, 1987; Huggel et al., 2002), lake volume is difficult to directly obtain by means of satellite remote sensing approach. Currently, due to the easy availability of area information from remote sensing images, the volume of glacial lakes is generally estimated using the developed empirical formulas to connect glacial lake area and volume based on bathymetric data for a small number of glacial lakes (O'Connor et al., 2001; Huggel et al., 2002; Yao et al., 2014). However, the estimated volume may be inaccurate because of the unique geographical conditions of different glacial lakes (Cook and Quincey, 2015). Although the SETP region is an area with a high incidence of GLOFs (Sun et al., 2014; Zheng et al., 2021; Zhang et al., 2023), there have been few publicly available bathymetric data of glacial lakes and related research works. Previous bathymetric works in the Tibetan Plateau were carried out mainly for glacial lakes located in the Himalayas (LIGG/WECS/NEA, 1988; Geological Survey of India, 1995; Yamada, 1998; Mool et al., 2001; Sakai, 2003; Yamada, 2004; ICIMOD, 2011; Sakai, 2012; Yao et al., 2012; Wang et al., 2015; Haritashya et al., 2018; Sharma et al., 2018; Li et al., 2021). This is unfavorable to fully understand the morphology and optimal disaster prevention strategies of glacial lakes in the SETP region. In recent years, unmanned surface vessels (USVs) have developed rapidly (Liu et al., 2016), and have been widely used in certain scenarios, such as bathymetric map creation, transportation, environmental monitoring, and moraine surveys (Larrazabal and Peñas, 2016; Yan et al., 2010; Specht et al., 2019), owing to personnel safety and high flexibility in complex environments. Glacial lakes are mostly located at high altitudes and in harsh environments (Zhang et al., 2020), and USVs make the measurement of the underwater topography of glacial lakes safer, more convenient, and more accurate (Li et al., 2021).

In this study, we aim to complete an investigation of the potential GLOF hazard of an end moraine-dammed glacial lake,

Bienong Co ("Co" means "lake" in Tibetan) in the SETP based on field bathymetric data and remote sensing data using a multi-model combination method. First, the lake basin morphology of Bienong Co is modelled. Then, multiple components of the GLOF process chain, including initial mass movement from the mother glacier and lateral moraine slope, displacement wave generation and propagation in the lake, overtopping flow and erosion on the moraine dam, and subsequent downstream flooding were simulated. This study will assist the local government to understand the potential hazards of Bienong Co and serve as a reference for other scholars studying glacial lakes and GLOFs in the SETP region.

2 Study area

Bienong Co is located in the upper area of the Yi'ong Zangbo ("Zangbo" means "river" in Tibetan) watershed (30˚05' - 31˚03'N, 92˚52' - 95˚19'E) in the SETP (Fig. 1a). As a one-level tributary of the Parlung Zangbo and a two-level tributary of the Yarlung Zangbo (i.e., the Brahmaputra River), the Yi'ong Zangbo drains an area covering 13,533 km^2. The terrain is high in the west and low in the east with high mountains and valleys. The climate is warm and humid, featuring a mean annual precipitation of 958 mm and a mean annual temperature of 8.8 ℃ (Ke et al., 2013, 2014). There was 1,907.76 km^2 glacier coverage, and 105 moraine-dammed glacial lakes with a total area of 16.87 km^2, in 2016 (Duan et al., 2020). Seven glacial lakes in the watershed, including Bienong Co, were considered to have high GLOFs potential (Duan et al., 2020), of which Jinwu Co collapsed on June 26, 2020 (Zheng et al., 2021). As of 2021, there have been three recorded large GLOF events in the basin, all of which caused very significant damage to infrastructures in the downstream region (Sun et al., 2014; Yao et al., 2014; Zheng et al., 2021) (Fig. 1b). Bienong Co is an end moraine-dammed lake constrained by the mother glacier (Mulang Glacier) on the south and a massive unconsolidated terminal moraine dam on the northwest (Fig. 1c). The elevation of the water surface in 2021 was 4,745 m covering an area of 1.15 ± 0.05 km^2 that has experienced less significant changes. The Mulang Glacier had an area of 8.29 ± 0.22 km^2 and a mean surface slope of ~18.28˚, which has also remained a largely unchanged area over the last 45 years. However, the glacier ablation zone experienced a thinning process of 6.5 m/a. The flow of Bienong Co converges into Xiong Qu ("Qu" means "river" in Tibetan), which is one of the two main tributaries of the upper Yi'ong Zangbo (Fig. 1b). The flow channel from Bienong Co to the confluence of Xiong Qu and Song Qu (another main tributary of the upper Yi'ong Zangbo) stretches ~53 km, with a river longitudinal drop ratio of 14.48‰. There are 18 settlements and 13 bridges densely distributed along the flow channel, as well as a large amount of agricultural land. In addition, the Jiazhong Highway extends closely along the river (Fig. 1d).

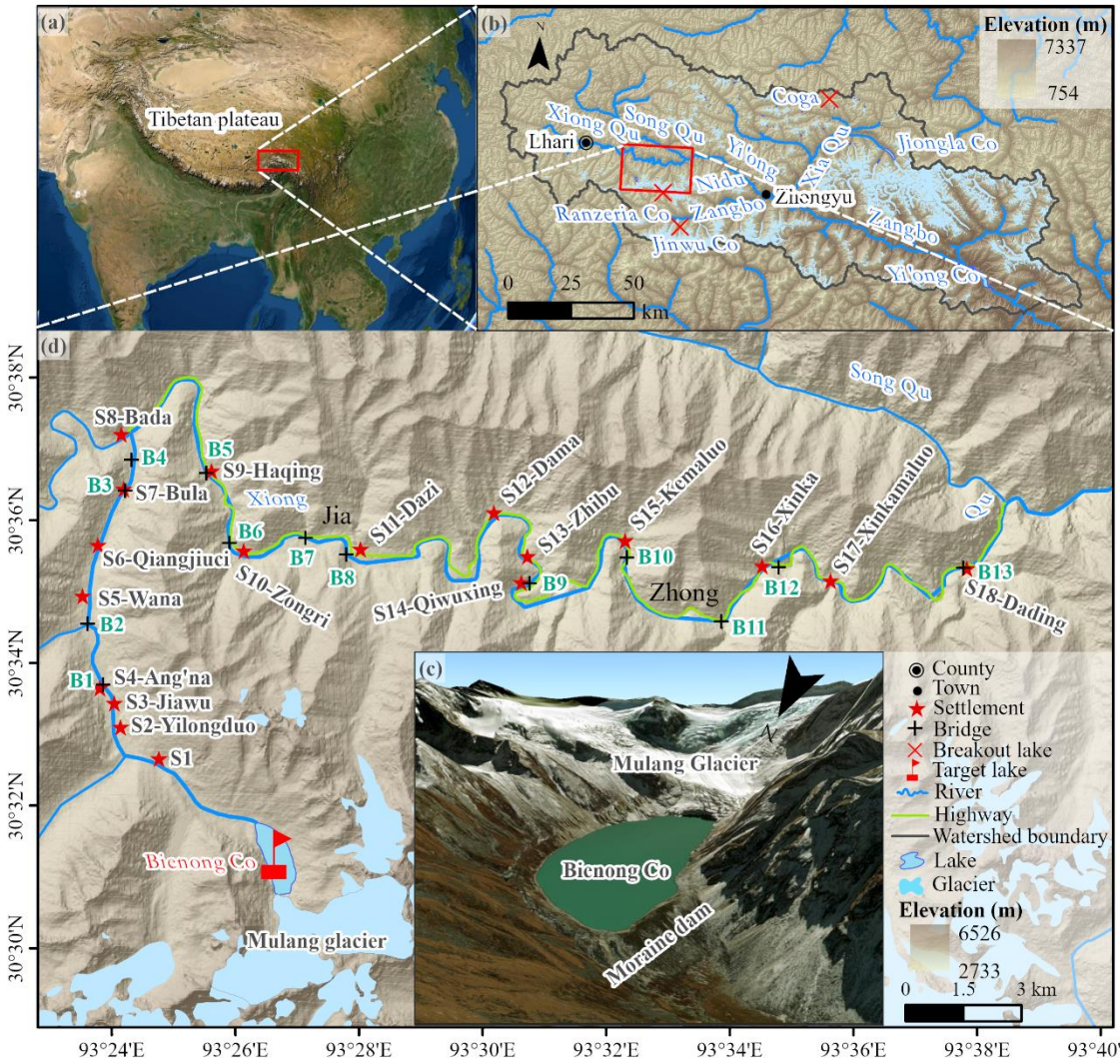

Figure 1. Overview of the study area. (a) The location of the Yi'ong Zangbo watershed, (b) the location of Bienong Co, (c) a close view of Bienong Co, and (d) the distribution of settlements, as well as bridges, within ~53 km downstream of Bienong Co. The background of Fig. 1a and c is a MapWorld image, based on which settlements, bridges, and the Jiazhong Highway along the flow channel were identified. The background of Fig. 1b and d is the Advanced Land Observing Satellite's (ALOS) mission Phased Array type L-band Synthetic Aperture Radar (PALSAR) Digital Elevation Model (DEM).

The area of Bienong Co has remained basically stable in the past 40 years, but its area of 1.15 ± 0.05 km^2 in 2021 was almost twice the size of the two nearby outburst moraine-dammed glacial lakes, one of which is Jinwu Co (Zheng et al., 2021) and the other is Ranzeria Co (Sun et al., 2014; Zhang et al., 2022), which were located just 24 km and 9 km southeast of Bienong Co, respectively. The moraine dam of Bienong Co has an average height of 72 m, enclosing a lake volume of 65.2×10^6 m^3, accounting for 64% of the total (Fig. 2e). Overall, the greater is the volume of water retained in the lake, the greater is the volume of water available for potential flooding (Westoby et al., 2014), and the greater is the hazard caused by GLOFs. GLOFs are highly complex phenomena, each of which constitutes a distinctly unique event with characteristics determined by the triggering mechanism, lake hypsometry, geometry, composition, and structural integrity of the moraine dam, as well as the topography and geology of the flood path (Westoby et al., 2014). Studies of historical GLOFs reveal that the most common cause of glacial lakes' failure in the Himalayas is mass movement (snow, ice, and/or rock) entering lakes (Richardson and Reynolds, 2000; Wang et al., 2012a; Emmer and Cochachin, 2013; Worni et al., 2014), and subsequently overtopping and eroding of the moraine dam (Risio et al., 2011). Bienong Co is directly connected to the Mulang Glacier, whose ablation zone is defined as the mother glacier tongue in this study, and has an average slope of 20° with well-developed ice crevasses (Fig. 2a and b). Lv et al., (1999) proposed that a slope of mother glacier tongue greater than 8° is

conducive to the occurrence of ice avalanche. In the context of global warming, glacial meltwater can lubricate the glacier itself, increasing the likelihood of overhanging ice sliding into the lake (Wang et al., 2015). Therefore, ice disintegration from the Mulang Glacier could be a potential trigger for GLOFs of Bienong Co. In addition, the GLOF of Jinwu Co was caused by an initial moraine landslide with a slope range of 30˚ - 45˚ on the left side (Zheng et al., 2021). Bolch et al. (2011) and Rounce et al. (2016) both reported that non-glacierized areas around a lake with a slope > 30° are potential rock fall, landslide, or other solid mass movement regions. There are multiple locations with lateral moraines around Bienong Co that fit into this slope range (Fig. 2c, d, and e). Therefore, lateral moraine landslides could also be a potential trigger for Bienong Co's GLOF.

Dam characteristics, such as dam geometry (freeboard, width-to-height ratio, distal face slope), dam material properties, and ice-cored moraine conditions, govern the stability of the dam (Huggel et al., 2004; Prakash and Nagarajan, 2017; Wang et al., 2011a). Freeboard refers to the vertical distance between the lake level and the lowest point on the dam crest, which reflects the minimum requisite wave amplitude for the occurrence of overtopping, and a higher freeboard is not conducive to the occurrence of overtopping (Emmer and Vilímek, 2014). A natural outlet with a width of ~50 m is in the right of the dam (facing downstream) (Fig. 2e and f), indicating that the freeboard of Bienong Co is 0 m, which signals the high potential for overtopping of the lake. The moraine dam is ~520 m wide and the height is variable with an average height of ~72 m, and the width-to-height ratio is 7.2 (Fig. 2e). According to the thresholds favoring GLOFs of dam widths smaller than 60 m proposed by Lv et al. (1999) and width-to-height ratios smaller than 0.2 proposed by Huggel et al. (2004), the moraine dam of Bienong Co is stable. However, the freeboard of 0 m and the distal facing slope of 35˚ are conditions that are conducive to GLOFs based on favorable thresholds of smaller than 25 m (Mergili et al., 2011) and larger than 20˚ (Lv et al., 1999). The moraine dam of Bienong Co is covered with vegetation, the surface layer is a larger particle size of the stone, and below the smaller particle size, the material is loose and poorly cemented, which is susceptible to destruction by water forces (Fig. 2e). The existence of ice core inside of the moraine dam is unknown, but there is no ice core in Jinwu Co's breached dam. The dam crest elevation of Bienong Co is 320 m higher than that of Jinwu Co. Additionally, McKillop and Clague (2007) argued that moraines with rounded surfaces and minor superimposed ridges are considered ice-cored, whereas narrow, sharp-crested moraines with angular cross-sections are interpreted as ice-free, and the dam of Bienong Co clearly fits the latter category. In aggregate, we consider that the potential threats to Bienong Co are mainly ice avalanches from the mother glacier and lateral moraine landslides.

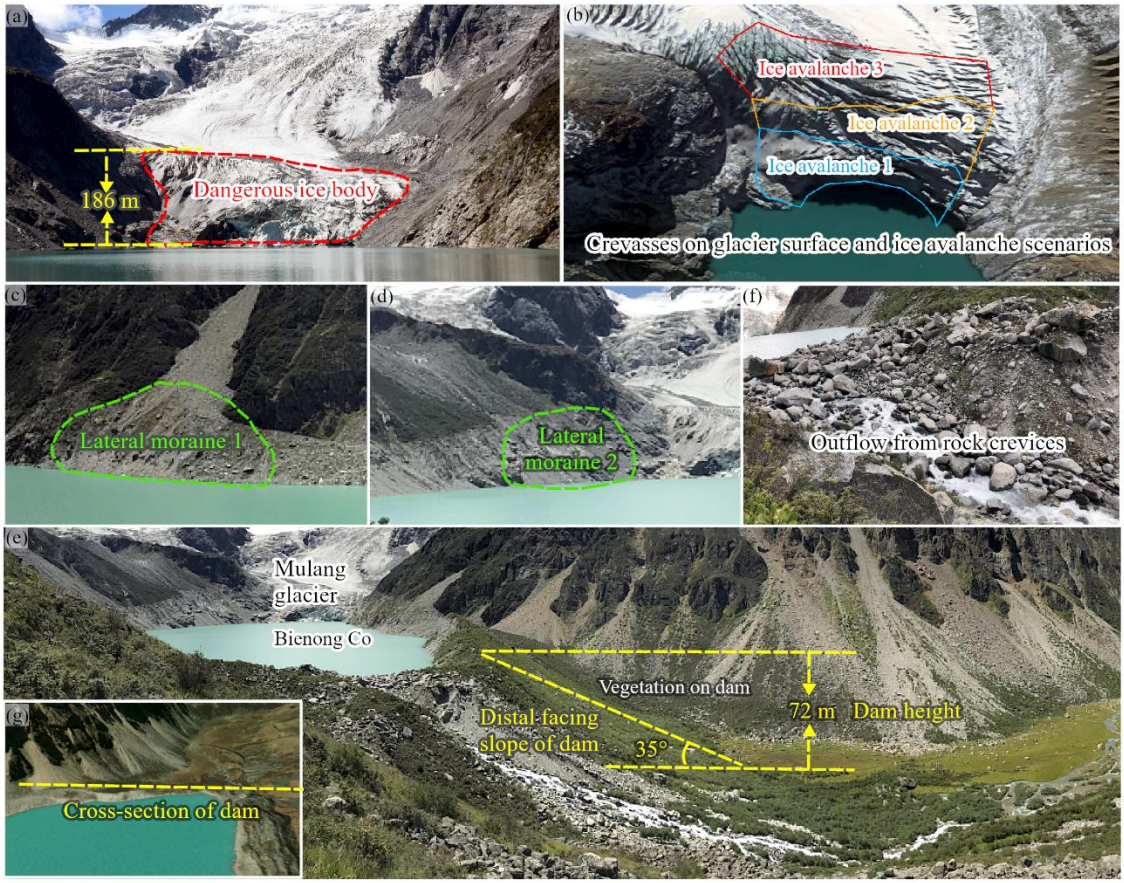

Figure 2. The hazard assessment of Bienong Co. (a) The connection condition of the Mulang Glacier and Bienong Co, (b) the crevasses on the glacier surface and the assumed ice avalanche scenarios of the Mulang Glacier, (c) and (d) the assumed lateral moraine location, (e) and (f) the moraine dam of Bienong Co, and (g) a cross-section of the moraine dam for statistical purposes. Fig. 2(b) and (g) are based on a MapWorld image, and the other photographs were taken by Xiaojun Yao and Qi Wang on August 27, 2020.

3 Methodology

3.1 Bathymetry and modeling

Lake bathymetric information is one of the most important inputs in the dynamic modeling of GLOFs, and can accurately reflect the topography of the lake basin below the water surface and used to calculate the potential flood volume released in different breach scenarios (Westoby et al., 2014). In this study, the depth data were obtained by a USV (APACHE 3) system, which consists of four main parts: the data acquisition module; the data transmission module; the positioning and navigation control module; and the power module (Li et al., 2021) (Fig. 3a and b). The USV system has a draft of 10 cm, which is smaller than the inflatable kayak used in previous investigations (Haritashya et al., 2018; Sattar et al., 2019, 2021). The D230 Single-Frequency Depth Sounder mounted on the USV is designed to measure a range of 0.15 - 300 m with a depth resolution of 1 cm and a bathymetry error of ± 1 cm+0.1%×h (water depth). The sounder can operate at 200 kHz and a water temperature range of -30℃ - 60℃. Meanwhile, a real-time kinematic system enables precise positioning for the bathymetric position with a horizontal error of ± 8 mm, a vertical error of ± 15 mm, and a directional error of 0.2˚ on the 1 m baseline. Field measurements were carried out on August 27, 2020. We designed four longitudinal routes and 13 transverse routes prior to the survey, along which the USV-based measurement was conducted (Fig. 3c). The maximum speed of the USV can reach 8 m/s, and our survey was conducted at a speed of 2 m/s for a total route of 22.58 km in Bienong Co. Due to absence of any obstructions on the lake, such as ice or small islands, the high performance of the USV and the real-time monitoring,

the survey was accurately completed along the designed route. A total of 16,020 valid sounding points, essentially covering the entire glacial lake, were measured, which well fulfilled the data density requirement to model the lake basin topography (Fig.3c).

The bathymetric map was created within ArcGIS Pro software using the natural neighbor interpolation algorithm (Thompson et al., 2016; Haritashya et al., 2018; Watson et al., 2018). In addition, Surfer software was employed to simulate the 3D morphology of Bienong Co's lake basin. Lake capacity can be understood as the volume of water storage below a certain water level, which is the volume between a certain spatial curved surface and a certain horizontal surface (Shi et al., 1991). In this study, the volume of Bienong Co was obtained by multiplying the depth data and map resolution (5 m) as follows:

$$V = \sum_{i=1}^{n} H_i \cdot \lambda \tag{1}$$

where V is the volume (m^3) of Bienong Co; H_i is the depth (m) at the *i-th* pixel; n is the number of pixels in the lake area; and λ is the pixels resolution (m^2) of the bathymetric map.

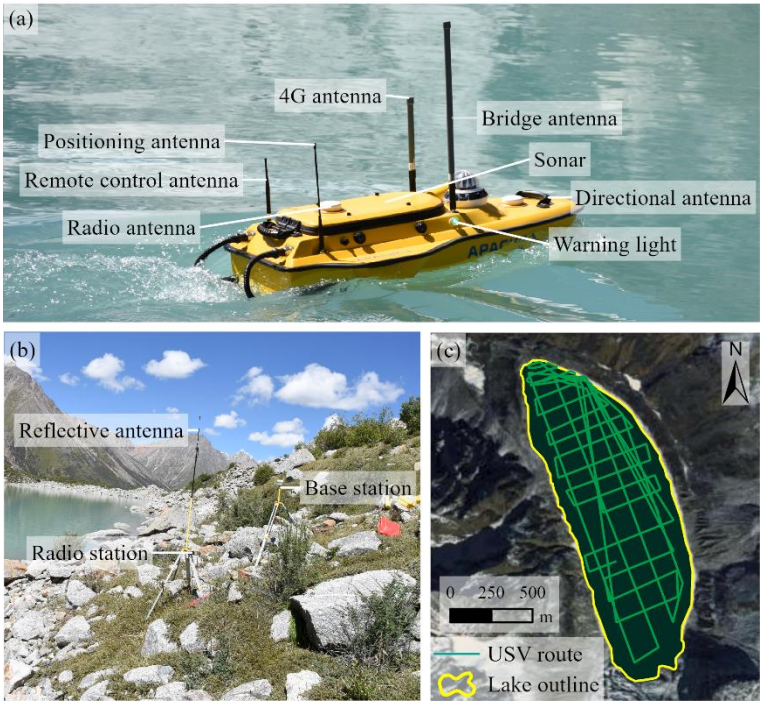

Figure 3. The bathymetry of Bienong Co. (a) The USV sampling equipment in water and (b) on land; (c) the sampling path of USV on Bienong Co covering the base map of the MapWorld image. Photographs were taken by Xiaojun Yao on August 27, 2020.

3.2 Potential GLOF modeling

Emmer and Vilímek (2014) and Haeberli et al. (2001) suggested that the assessment of glacial lake hazards should be carried out based on a systematic and scientific analysis of lake types, moraine dam characteristics, outburst mechanisms, downstream processes in the river valley, and possible process cascades. The methodology used in this study refers to the GLOFs process chain proposed by Worni et al. (2014), which has been utilized by Somos-Valenzuela et al. (2016) and Lala et al. (2018) to study Imja Tsho in Nepal and Palcacocha and Huaraz lakes in Peru, respectively. In this study, we aim to depict potential GLOFs induced by ice avalanches originating from the Mulang Glacier (Fig. 2a and b) and landslides from the lateral moraine (Fig. 2c and d), and assess potential inundation in the downstream region. The wave resultant from material entering Bienong Co might overtop the moraine dam and initiate an erosive breaching process, releasing considerable amounts of water and debris into the downstream flow channel (Somos-Valenzuela et al., 2016). Three models were used to simulate the GLOFs process chain: the RAMMS model was used for simulation of potential mass movement

(Christen et al., 2010); the BASEMENT model was used to simulate the displacement wave in the lake; and the Heller-Hager model was used as a calibration for BASEMENT's results. The BASEMENT model was also adopted to simulate the dynamic breaching process of the moraine dam, the propagation of the flood wave, and the inundation downstream. In the next sections, simulation methods for ice avalanches and landslides, displacement waves in lakes, overtopping flow and erosion on the moraine dam, and downstream inundation are described.

3.2.1 Triggers determination and simulation

Ice avalanches are the most common GLOFs trigger in Tibet in China (Yao et al., 2014; Liu et al., 2019). Mass movements into lakes generate impulse waves that may produce overtopping flow scouring and erosion of moraine dams, or disrupt the hydrostatic pressure-bearing capacity of moraine dams. Based on a survey of the environment surrounding Bienong Co, ice avalanches from the Mulang Glacier and lateral moraine landslides at two locations were selected as potential triggers for GLOFs. Wang et al. (2012) defined the volume of dangerous glaciers as the volume from the location of the abrupt changing slope to the glacier termini or the volume of the glacier tongue where ice cracks are well developed. We adopted the latter, i.e., the crevasse-developed ice body of the Mulang Glacier shown in the MapWorld image with a surface area of 0.19 km^2 was selected as the potential ice avalanche source of Bienong Co (Fig. 2a). For convenience of subsequent description, we name it Scenario A. The elevation difference between the top of the dangerous ice body and the lake surface was measured to be approximately 155 – 208 m based on ALOS PALSAR DEM. We divided the dangerous ice body into three parts according to elevation range to simulate subsequence processes from ice avalanches of different magnitudes (ice avalanche 1, 2, and 3 in Fig. 2b). Scenario A1 was defined as a low-magnitude trigger, and the ice body at an elevation below 4,844 m yields a release area of 0.05 km^2 with the maximum and average elevation differences of 99 m and 75.8 m from the lake surface, respectively. Scenario A2 was defined as a moderate-magnitude trigger, ice body at elevation below 4,889 m yields a release area of 0.11 km^2 with the maximum and average elevation differences of 144 m and 102.7 m from the lake surface, respectively. Scenario A3 was defined as an extreme-magnitude trigger, and the total ice body of crevasse with an area of 0.19 km^2 was set as a release area, with the average elevation difference between glacier surface and lake surface of 131 m. In the above three cases, we assumed that the release depths of ice avalanches are the average elevation differences from the glacier surface to the lake surface, i.e., the glacier is supported by flat bedrock located at the height of the lake water table.

Lateral moraine landslides as a GLOFs trigger are not common on the Tibetan Plateau, but the GLOF of Jinwu Co in 2020 was caused by a lateral moraine landslide (Liu et al., 2021; Zheng et al., 2021), and thus was taken as a trigger of the potential GLOF for Bienong Co. Two areas of lateral moraine within the slope range of 30˚ - 45˚ were selected as potential landslide sites, one of which is located on the left bank (in this study, the left and right sides are defined in a downstream-oriented manner) of Bienong Co, near the moraine dam with an area of 0.015 km^2, and we named it Scenario B (Fig. 2c). Another is located on the right bank, near the mother glacier with an area of 0.024 km^2, we named it Scenario C (Fig. 2d). The two sites are at different distances from the moraine dam and we set three different release depths of 2 m (Scenario B1 and C1), 5 m (Scenario B2 and C2), and 10 m (Scenario B3 and C3) for each release area as low-, moderate-, and extreme-magnitude trigger, respectively. Therefore, a total of two different types, three different locations, and nine different magnitudes of materials were designed to enter the lake as potential triggers for GLOFs in this study. The above design fully considers the impact of triggers on Bienong Co under different magnitudes, and the results are used as the input for the subsequent disaster chain simulation.

In this study, ice avalanches and lateral moraine landslides of Bienong Co were modeled using the Avalanche module of the Rapid Mass Movement Simulation RAMMS model (Bartelt et al., 2013), which has been successfully used for simulating triggers of GLOFs (Somos-Valenzuela et al., 2016; Lala et al., 2018; Sattar et al., 2021). RAMMS adopts the Voellmy-Salm finite volume method to solve depth-averaged equations governing mass flow in two dimensions (Christen et al., 2010). Based on the basic inputs of DEM, the initial release area and depth, the calculation domain, the friction

parameters μ (the velocity-independent dry Coulomb) and ξ (velocity-dependent turbulent friction terms), the outputs of runout distances, flow height, and flow velocity can be calculated. In addition, the time series of material entering the glacial lake can serve as the input condition for subsequent simulations. For this study case, the initial release area was determined by combining the MapWorld image with a spatial resolution of 0.5 m (https://www.tianditu.gov.cn/) and ALOS PALSAR DEM with a spatial resolution of 12.5 m (https://asf.alaska.edu/data-sets/derived-data-sets/alos-palsar-rtc/alos-palsar-radiometric-terrain-correction/). Values of μ=0.12, ξ=1,000 m s^{-2}, and ρ=1,000 kg m^{-3} for ice avalanche and ρ=2,000 kg m^{-3} for landslide were used, which agree with values used in previous GLOF-producing avalanche models (Schneider et al., 2014; Somos-Valenzuela et al., 2016).

3.2.2 Hydrodynamic wave simulation

Processes following mass movement entering the lake, such as the generation and propagation of displacement wave, the overtopping flow and erosion on the moraine dam, and downstream inundation were modeled using the BASEMENT model v2.8.2 (Vetsch et al., 2022), developed by the Laboratory of Hydraulics, Glaciology and Hydrology (VAW), ETH Zurich. BASEMENT is both a hydrodynamic model and a sediment transport model, making it well suited to model much of the GLOF process chain (Worni et al., 2014). It solves the 2D shallow water equation (SWE) in combination with sediment transport equations, primarily the Shields parameters and the Meyer-Peter and Müller (MPM) equations (Vetsch et al., 2022). The simulation of hydrodynamic waves in the lake is performed using the 2D modeling of BASEMENT based on unstructured grids. The BASEmesh plugin for QGIS (QGIS Development Team, 2016) developed by BASEMENT greatly facilitates the generation of mesh. The lake bathymetry data were entered into DEM with a spatial resolution of 5 m using ArcGIS Pro software to reflect the lake basin topography. The triangular irregular network (TIN) within the lake area was set to a maximum area of 500 m^2 to simulate the generation and propagation of hydrodynamic waves in the lake effectively and accurately. The input boundary conditions are time series of ice avalanches and landslides generated by RAMMS model. In each time period, the RAMMS calculates the total amount of sediment, and the inflow rate can be determined by calculating the difference of sediment entering the lake at two time points. Pure rock landslides have been investigated with densities ranging from 1,950 kg m^{-3} to 2,200 kg m^{-3} (Wang et al., 2017), and most ice-dominated avalanches have densities of approximately 1000 kg m^{-3}. In this study, the ice avalanche density was set as 1,000 kg m^{-3}, and the landslide density was set as 2,000 kg m^{-3}. Since BASEMENT only accepts water as an inflow, this difference due to density is considered by expanding the landslide material entry rate by a factor of two (i.e., 1,000 kg m^{-3} of water is equivalent to 1,000 kg m^{-3} of ice avalanche volume, and only 500 kg m^{-3} of landslide material), which is the usual approach used in the simulation process (Byers et al., 2018 and 2020).

It was shown that the 2D SWE used by the BASEMENT model inherently leads to excessive wave attenuation. The Heller-Hager model (Heller et al., 2009) is a combination of analytical and empirical equations used to simulate impulse wave generation, propagation, and run-up from the movement of material entering a lake. Although the approach relies on simplifying measurements about lake geometry, it has been used to successfully simulate multiple real events and performs well in characterizing impulse waves within lakes, making it a simple, but useful, calibration measure for more complex hydrodynamic models (Somos-Valenzuela et al., 2016). BASEMENT simulated waves are usually considered more accurate when they are of the same order of magnitude as Heller-Hager waves; however, when they are not, the mass entry rate is varied by adjusting the inflow hydrograph and boundary width to match the amplitude of the Heller-Hager empirical model near the dam of the initial wave trajectory (Byers et al., 2018; Lala et al., 2018). The Heller-Hager model simulates waves in two cases: (a) with longitudinal impacting slide and confined transverse wave propagation; and (b) with the slide impacting across the reservoir and completely free radial wave propagation. In present study, ice avalanches belong to case (a), and landslides belong to case (b). Compared to case (a), the impulse wave (its amplitude and energy) in case (b) decreases more rapidly because it propagates over a larger area, and is accompanied by wave refraction and reflection.

3.2.3 Moraine dam erosion simulation

Abnormally high lake outflow is sufficient to destroy the surface protection layer of the outlet streambed and triggers vertical dam erosion. After the initial cut, more lake water will flow out, followed by an increase in sediment transport rate and a gradual widening of the rift. In this study, hydro-morphodynamic simulations of potential erosion-driven breach failures of Bienong Co were carried out by the BASEMENT model, which uses the Meyer-Peter and Müller (MPM) equation to characterize sediment transport, and estimates suspended and nudged mass fluxes by calculating the shear stress in the flow through the modified Shields parameter (Vetsch et al., 2022). The overtopping flow leading to erosion of the moraine dam is generated by the wave amplitude of the BASEMENT model calibrated by the Heller-Hager model. In the previous step, we adjusted the wave amplitude near the moraine dam in the BASEMENT model to be close to (difference within 1 m) that calculated by the Heller-Hager model by modifying the width of the upstream boundary. ALOS PALSAR DEM is the base data for the mesh generation of the moraine dam with the maximum TIN area of 200 m^2. We set a cross-section along the crest of the moraine dam (Fig. 2g), where moraine dam deformation, i.e., erosion, overtopping, as well as outflow discharges, were analyzed. The BASEMENT model provides both single-grain (MPM) and multi-grain (MPM-multi) algorithms to simulate material transport. The MPM-multi model simulates hiding and armoring processes that may lead to unrealistically low levels of erosion (Vetsch et al., 2022). The MPM model ignores these processes, however, which can lead to an overestimation of erosion. In this study, we applied the MPM-multi model to simulate bed-load transport of the moraine dam, which is composed of materials with different grain sizes. The specific grain size distribution was not measured, but was instead taken from an inventory of glacial lakes in the Indian Himalayas (Worni et al., 2013) that had performed well in recreating previous GLOFs in Nepal (Byers et al., 2020). Despite uncertainty in the actual grain size distribution, a similar GLOF modeling study in the Barun Valley (Byers et al., 2018) found little difference in simulated moraine erosion between the grain size distributions listed in Worni et al. (2013). The moraine dam of Bienong Co consists of a large grain cover with a thickness of approximately 0.5 m at the top and fine grain underneath, which is clearly visible on the side walls of the channel scoured by water (Fig. 2e). We set up two soil layers in the BASEMENT model to represent the above situation. The largest particle size (d_{50} = 180 mm) in the upper layer with a depth of 0.5 m, and the grain size distribution of the lower layer with a depth of 71.5 m (considering the mean height of moraine dam of 72 m), are consistent with Worni et al. (2013). Finally, a correction factor of 2.0 was used in the model to increase the rate of bed load transport. Values between 0.5 (low transport) and 1.7 (high transport) are generally realistic (Wong and Parker, 2006); whereas a value of 2.0 provides high sediment transport conditions (Somos-Valenzuela et al., 2016) to compensate for the lower erosion of the MPM-multi model.

3.2.4 Downstream impact analysis

The flow channel from Bienong Co to the convergence with Song Qu stretches ~53 km (Fig. 1d), along which 18 settlements, 13 bridges, and the Jiazhong Highway are distributed. In this study, the BASEMENT model was used to simulate the hydrodynamic behavior of potential GLOFs along the flow channel, and the hazard of floods was assessed by analyzing the inundation area, flow velocity, and flood arrival time at these settlements. The 2D model for an unsteady hydraulic simulation requires input of terrain data and boundary conditions. The terrain data were represented by a 2D mesh covering the entire flow area, which was obtained from ALOS PALSAR DEM. The mesh was also generated by the BASEmesh plugin of QGIS software, and the individual cell area for the main flow channel and other regions were set to 500 m^2 and 5,000 m^2, respectively, considering the accuracy requirements of the simulation and the computational efficiency of the model. Friction of the river channel to a given flow was determined by the Manning's roughness coefficient (Coon, 1998), which is dependent on the land use and land cover of the modeling river channel in the study area. In this study, the GLC10 LULC product (http://data.ess.tsinghua.edu.cn/fromglc10_2017v01.html) with a spatial resolution of 10 m was used to obtain the value of Manning's N in the flow channel. The upstream boundary is the outflow hydrograph from the moraine

dam simulated by the BASEMENT model. The downstream boundary is the water level-discharge relationship of the cross-section in the downstream boundary of the simulation area, and was estimated by the critical depth method (Byers et al., 2018).

4 Results

4.1 Morphology and lake volume estimation of Bienong Co

The basin morphology of Bienong Co was modeled based on the TIN grid created by the field depth data (Fig. 3). Apparently, this lake has a relatively flat basin bottom, and both flanks are deep (Fig. 4). Similar to most glacial lakes (Yao et al., 2012; Zhou et al., 2020), the slope of the lake shores near the glacier is steeper than that near the moraine dam. The water depth profile from the moraine dam to the mother glacier shows that the depth of the lake reaches a maximum of ~181 m at approximately 1,000 m from the moraine dam, corresponding to a slope of 11.3˚. The depth remains stable at the distance of 1,000 m to 1,500 m from the moraine dam, and the distance from the Mulang Glacier to the deepest point of the lake is 600 m with a slope of 16.5˚. A depth profile facing the moraine dam from the left bank to the right bank shows that the left side is steeper than the right side. The glacial lake reaches its deepest point at 200 m from the left shore with a slope of 43.4˚, then remains flat to 430 m, and the distance between the bottom and right shore is 273 m with a slope of 32˚. The volume of Bienong Co, calculated using the surface elevation and the lake bed derived from the TIN grid, was approximately 102.3×10^6 m^3 in 2020, which is a generally accurate estimate of the magnitude of this moraine-dammed lake.

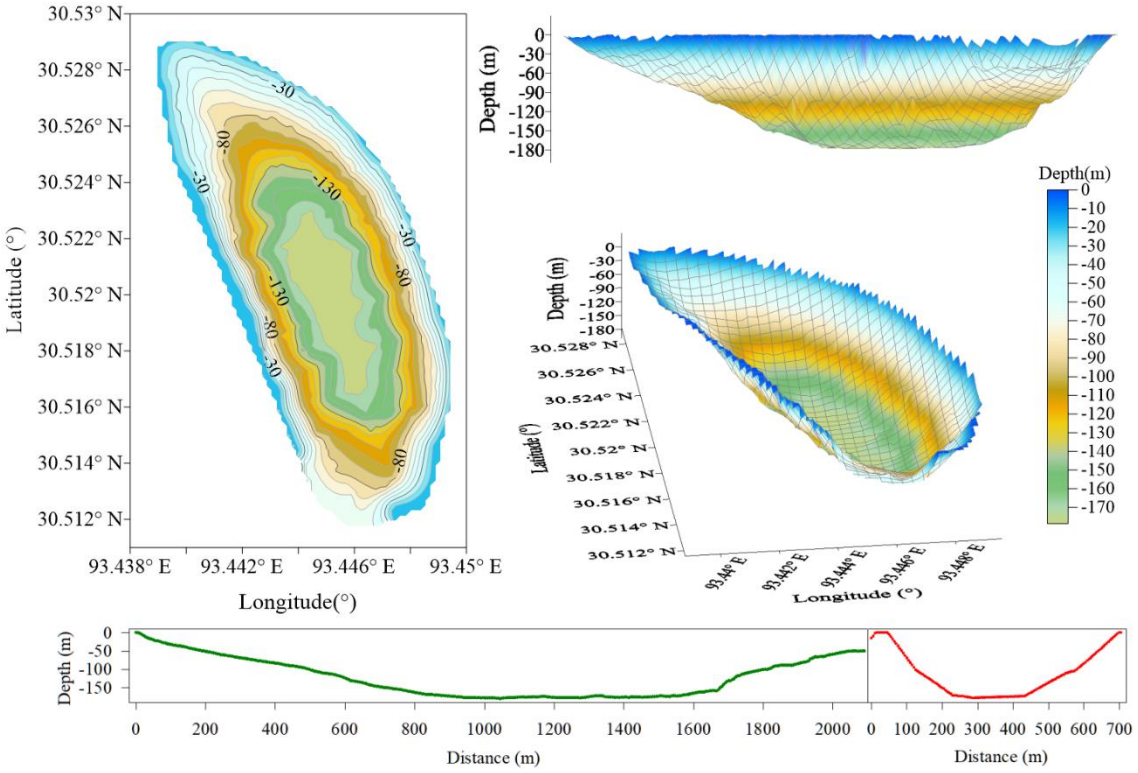

Figure 4. Morphology modeling of Bienong Co in 2020, and equal-scale profiles of distance and depth from the moraine dam to the Mulang Glacier (green line) and from the left shore to right shore (red line).

4.2 Potential GLOFs modeling

4.2.1 Ice avalanches and lateral moraine landslides

As calculated by RAMMS, the volume of ice avalanches entering Bienong Co for Scenarios A1, A2, and A3 are 3.8 × 10^6 m^3, 4.9 × 10^6 m^3 and 5.8 × 10^6 m^3 (Fig. 5a), respectively. Most of the materials enter the lake within approximately 120 s. Based

on the area of ~1.15 km^2 in 2021, the above three scenarios could result in a rise of approximately 3.3 m, 4.2 m, and 5.1 m in the lake surface, respectively. Material volumes entering the lake by both landslides are much smaller than those of the ice avalanches (Fig. 5b and c). Scenarios B1, B2, and B3 and C1, C2, and C3 dump 0.03 × 10^6 m^3, 0.09 × 10^6 m^3, and 0.17 × 10^6 m^3, and 0.06 × 10^6 m^3, 0.15 × 10^6 m^3, and 0.30 × 10^6 m^3 of material into the lake, respectively. The time for materials entering the lake is less than in Scenario A, with Scenario B being completed in approximately 10 s and Scenario C in approximately 15 s.

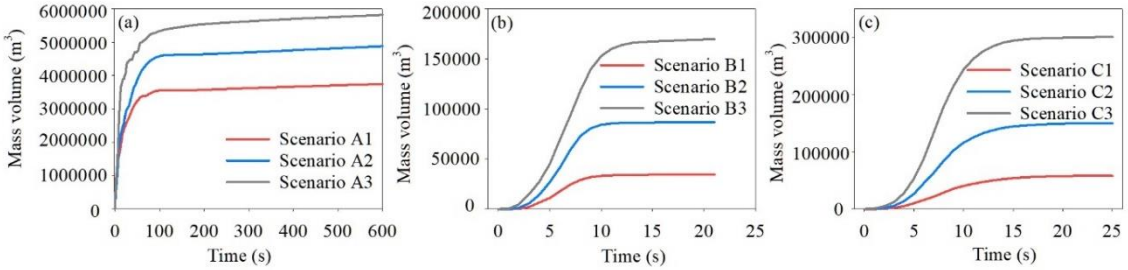

Figure 5. Volume of material entering Bienong Co for different (a) ice avalanche scenarios and (b) and (c) landslide scenarios.

The impact area caused by material entering the lake differs for different scenarios. The impact zones caused by Scenarios A1, A2 and A3 are 0.27 km^2, 0.31 km^2, and 0.38 km^2, with horizontal distances of 549 m, 629 m, and 752 m from the upper boundary, respectively (Fig. 6). In contrast, each of these three scenarios for Scenarios B and C result in a relatively small impact zone, with Scenario C3 being the largest at 0.14 km^2 and Scenario B1 being the smallest at 0.04 km^2. Scenarios A1, A2, and A3 produce maximum flow heights of 39.5 m, 46.2 m, and 53.5 m, and average flow heights of 12.2 m, 14.6 m, and 12.3 m in the impact area, respectively. The maximum flow height range for Scenarios B1, B2, and B3 is 6.8 - 14.6 m, and the average flow height range is 1.8 - 3.5 m. The maximum and average flow height ranges for Scenario C1, C2, and C3 are 5.7 - 29.2 m and 2.0 - 4.7 m, respectively (Fig. 6). The maximum flow velocities for Scenarios A1, A2, and A3 are 34.9 m/s, 43.1 m/s, and 51.4 m/s, with average flow velocities of 11.1 m/s, 12.3 m/s, and 16.8 m/s, respectively. The maximum and average flow velocities for Scenarios B1, B2, and B3 and C1, C2, and C3 are in the range of 21.3 - 33.6 m/s and 8.5 - 14.2 m/s, respectively (Fig. 6).

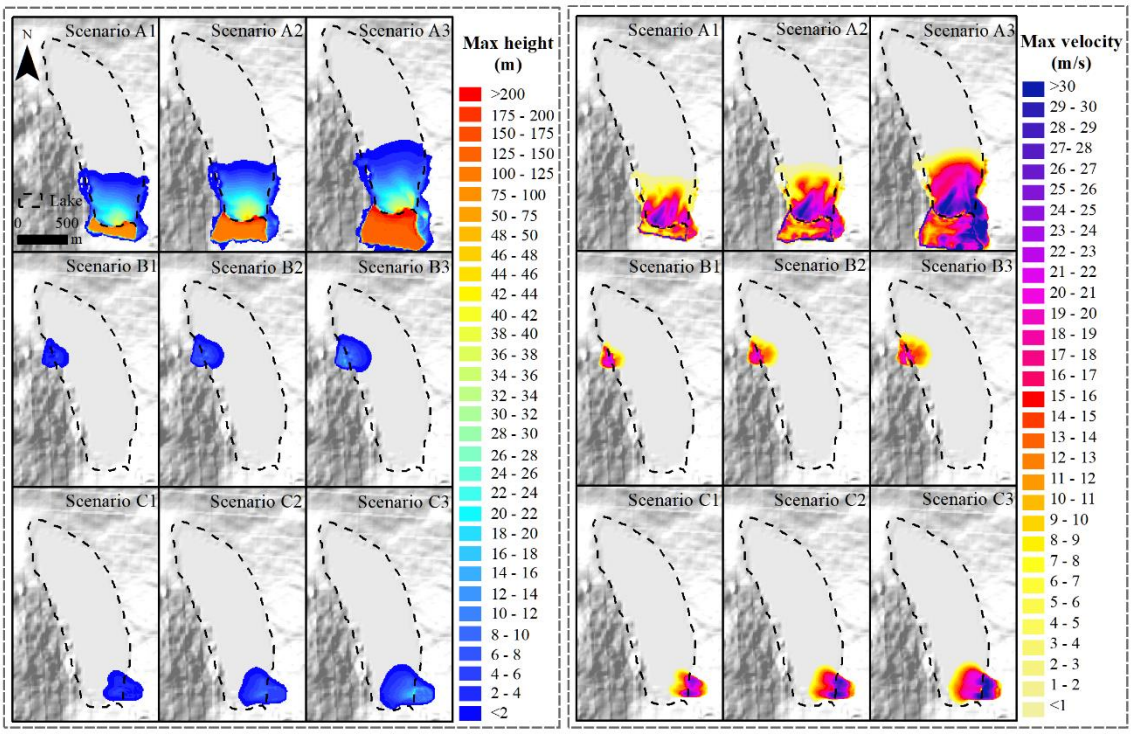

Figure 6. Maximum flow height (left) and maximum flow velocity (right) for different ice avalanches and landslides

scenarios.

4.2.2 Generation and propagation of displacement waves

By counting material volumes of ice avalanches and landslides entering Bienong Co at different time periods based on the RAMMS model, we derived the time series of the material-entering rate, as shown in Fig. 7. Compared to Scenarios A2 and A3, Scenario A1 has the highest peak flow rate of 439,952.57 m^3/s, but it decreases rapidly after reaching the peak within 2 s of the ice avalanche, i.e., the ice avalanche occurs in a moment. Scenarios A2 and A3 exhibit obvious fluctuations in the process of ice avalanches into the lake, with sub-peaks in both scenarios that are comparable to the first peak, after which the flow rates still possess strong fluctuations. The peak and sub-peak flow rate of Scenario A2 and A3 are 263,922 m^3/s and 238,086 m^3/s and 386,359 m^3/s and 373,449 m^3/s, respectively, both occurring at the 2nd and 8th seconds of the ice avalanche. This is because the ice avalanches of Scenarios A2 and A3 are further away from the lake than Scenario A1, and total volumes of ice avalanches are larger than Scenario A1, and thus they undergo a more complex process when they enter the lake. The process of landslide material entering the lake is simpler in Scenarios B and C. The peak flows increase sequentially from Scenarios B1 and C1, B2 and C2, to B3 and C3, with peak values of 50,849 m^3/s and 92,529 m^3/s for Scenarios B3 and C3, respectively. The peak flow for Scenario B3 is approximately 3.8 times that of Scenario B1, and that of Scenario C3 is 6.5 times that of Scenario C1, respectively. The peak flows for the six scenarios of Scenarios B and C occur in the range of 6 - 8 s seconds (Fig. 7).

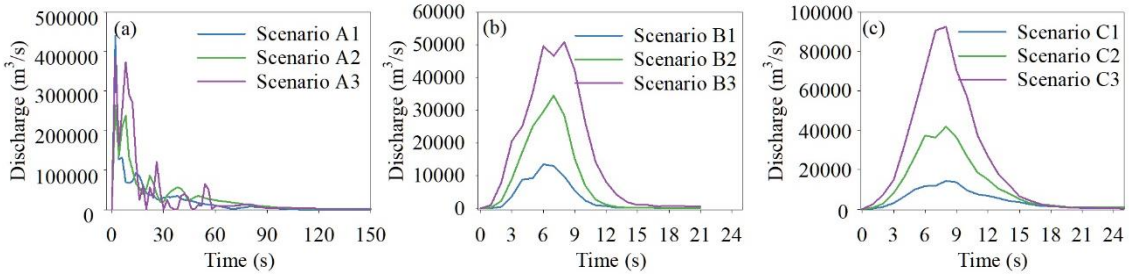

Figure 7. Time series of material entry into the lake for different ice avalanche and landslide scenarios.

The time-volume relationships of materials entering a lake have important effects on the generation and propagation of displacement waves in the lake. Ice avalanche scenarios (A1, A2, and A3) have a much greater impact on Bienong Co than the two landslide scenarios (B1, B2, B3, C1, C2, and C3) because the assumed release volume of ice avalanches is much greater than that of landslides. The wave height near the moraine dam is the result of the BASEMENT model calibrated by the Heller-Hager model. By adjusting the inflow boundary's width, we made the BASEMENT model produce wave amplitudes near the dam with a difference smaller than 1 m of those calculated by the Heller-Hager model, which is important for subsequent simulations, although the maximum wave amplitude in the lake is exaggerated.

In Scenario A, displacement waves propagate straight from the glacier to the moraine dam, and arrive at the vicinity of the moraine dam at approximately 70 s. Scenarios A1, A2, and A3 produce the highest wave amplitudes in the lake of 35.2 m, 39.0 m, and 66.4 m, respectively, and wave amplitudes near the moraine dam of 17.1 m (72 s), 20.2 m (74 s), and 25.2 m (72 s), respectively (Fig. 8). Compared with Scenario A, the wave amplitudes of Scenarios B and C are markedly lower. In Scenario B, a landslide occurs at the left shore of Bienong Co near the moraine dam (Fig. 2c). Displacement waves first propagate to the opposite shore in a perpendicular direction to the inflow boundary, and then they propagate to the moraine dam with the expansion. The maximum wave amplitudes in Bienong Co of Scenarios B1, B2, and B3 are 6.5 m, 14.1 m, and 18.0 m, respectively, and the wave amplitudes near the moraine dam are 1.2 m, 3.0 m, and 5.3 m, respectively (Fig. 8). The landslide in Scenario C occurs on the right bank of Bienong Co near the glacier, in the same manner as that in Scenario B, in which waves propagate to the opposite bank first after materials enter the lake, with the maximum wave amplitudes of 4.8 m, 9.6 m, and 24.7 m for Scenarios C1, C2, and C3. Unlike Scenario B, displacement waves in Scenario C cross the entire lake,

reaching the moraine dam with wave amplitudes of 0.6 m, 2.2 m, and 4.9 m near the moraine dam, respectively (Fig. 8). Therefore, although the landslide volume of Scenario C is larger than that of Scenario B, wave amplitudes near the moraine dam are smaller than those of Scenario B.

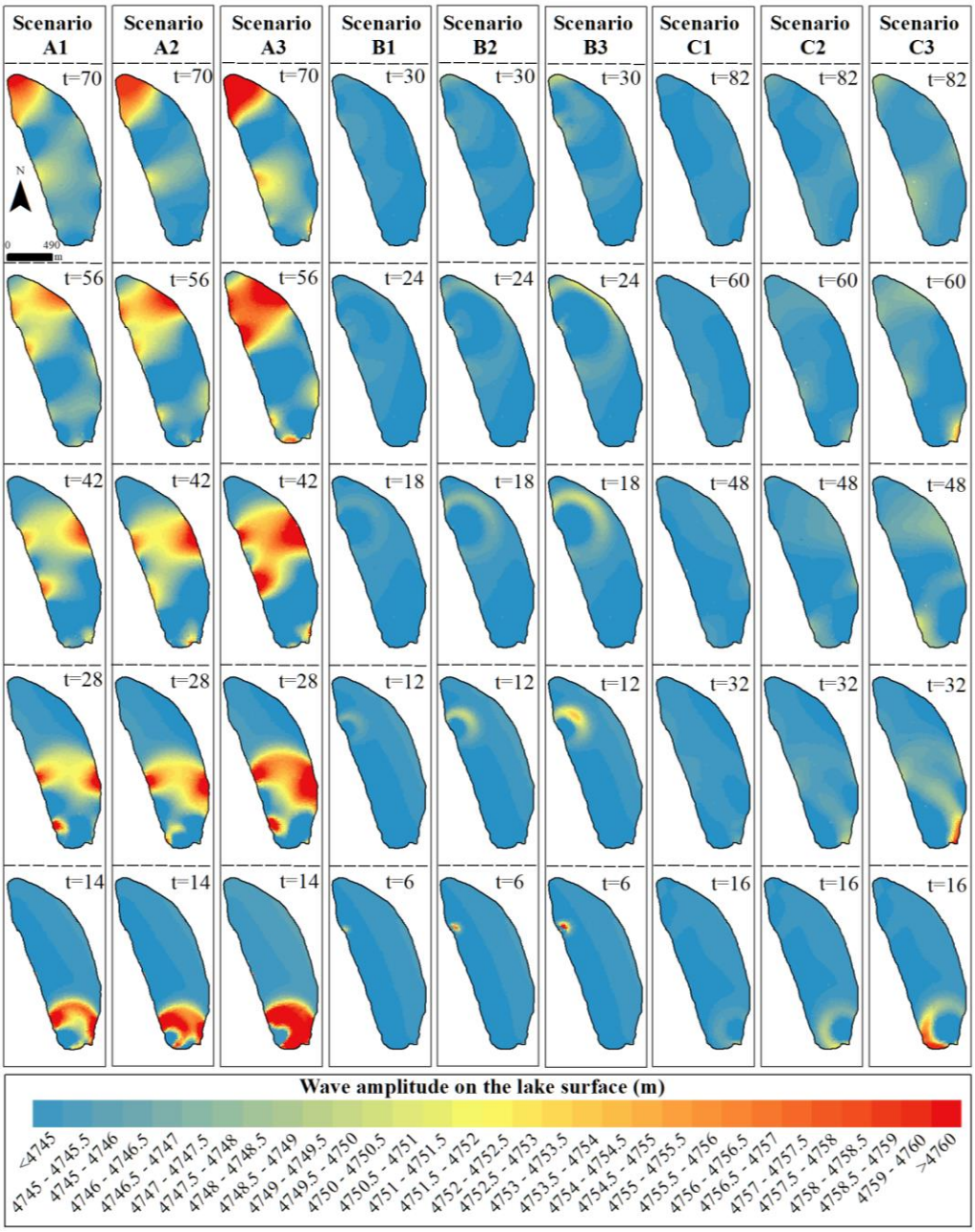

Figure 8. Propagation of displacement waves in the lake for different ice avalanches and landslide scenarios.

4.2.3 Overtopping flow and erosion on the moraine dam

Since the freeboard of the moraine dam is 0 m, the occurrence of overtopping flow is inevitable in all scenarios, but there are differences in magnitude. In Scenarios A1, A2, and A3, peak discharges at breaches of the moraine dam are 4,996 m^3/s, 7,817 m^3/s, and 13,078 m^3/s, corresponding to a total released volume of 24.1×10^6 m^3, 25.3×10^6 m^3, and 26.4×10^6 m, respectively (Fig. 9). Discharges at the moraine dam stabilize after ice avalanches enter Bienong Co at approximately 18,000 s, 10,800 s, and 7,200 s, respectively. Therefore, the erosion of the moraine dam and the total volume of water lost in the lake were counted based on the above time points. The moraine dam is eroded by enormous discharge output in Scenarios A1, A2, and A3, forming breaches. Due to the similar volume of released water, the depth of the breach is slightly different for Scenarios A1, A2, and A3, which are 19.0 m, 19.1 m, and 19.3 m, respectively (Fig. 10). Moreover, the peak discharge is

quite different for the three scenarios, resulting in different breach widths of 295.0 m, 339.4 m, and 368.5 m, respectively. Scenarios B1, B2, and B3 and C1, C2 and C3 resulted in overtopping flows of 0.6 × 10^6 m^3, 1 × 10^6 m^3, and 2.6 × 10^6 m^3, and 0.1 × 10^6 m^3, 0.9 × 10^6 m^3, and 3.4 × 10^6 m^3, respectively, in which only Scenarios B3 and C3 cause erosion of the moraine dam and form a breach. Discharges at the breach become stable beginning at 18,000 s following landslide material entry into the lake in Scenarios B3 and C3, with breach depths of 6.5 m and 7.9 m, and breach widths are 153 m and 169 m with peak discharges of 504 m^3/s and 733 m^3/s, respectively.

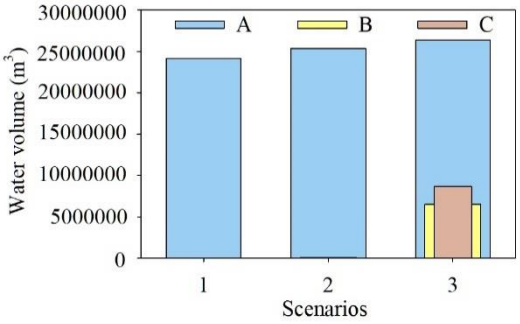

Figure 9. Discharge of water bodies in glacial lakes under different scenarios.

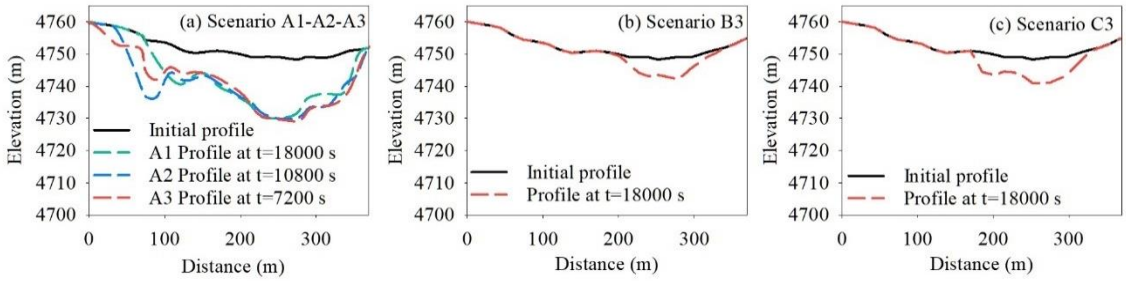

Figure 10. Erosion of the moraine dam under different conditions at the cross-section in Fig. 2g.

4.2.4 GLOFs impact in the downstream region

The hydraulic behavior of GLOFs in the flow channel immediately downstream of moraine dam to the convergence with Song Qu with the distance of ~53 km was simulated using the BASEMENT model. Due to the lack of reliable data on small baseflows in the flow channel, they were neglected in the simulation. Considering the propagation of floods in different scenarios, we assessed the propagation of GLOF in the downstream channel within 20 h from ice avalanche and landslide materials entry into the lake. Peak discharges at the breach outlet of Scenarios A1, A2, and A3 all occur approximately 600 s after the ice avalanche material enters the lake, and they are 4,996 m^3/s, 7,817 m^3/s, and 13,078 m^3/s, respectively, based on which floods all pass through 18 settlements in the downstream river in 20 h with the areas of 7.6 km^2, 8.0 km^2, and 8.5 km^2, as well as average water depths of 8.4 m, 9.1 m, and 10.0 m, respectively (Fig. 11). Scenarios B1 and C1 only have a small amount of overtopping flow from the lake (peak discharges of 106 m^3/s (after 40 s) and 12 m^3/s (after 50 s)), and fail to generate runoff downstream of the dam. Scenarios B2 and C2 produce very limited overtopping flow with peak discharges of 177 m^3/s (after 240 s) and 186 m^3/s (after 480 s), respectively, and outflows remain only within approximately 1 km downstream of the dam. Peak discharges at the breach outlet of Scenarios B3 and C3 are 504 m^3/s (after 240 s) and 733 m^3/s (after 480 s), yielding inundation areas of 1.7 km^2 and 2.2 km^2 with average water depths of 1.9 m and 2.4 m in the downstream region, respectively. Both GLOFs pass through the first eight settlements, but the flood of Scenario C3 flows farther (Fig. 11). Among the nine scenarios that we considered, only Scenarios A1, A2, A3, B3, and C3 caused GLOFs propagation in the downstream region with a far distance, in which Scenario A3 had the largest flood magnitude, and Scenario B3 had the smallest flood magnitude.

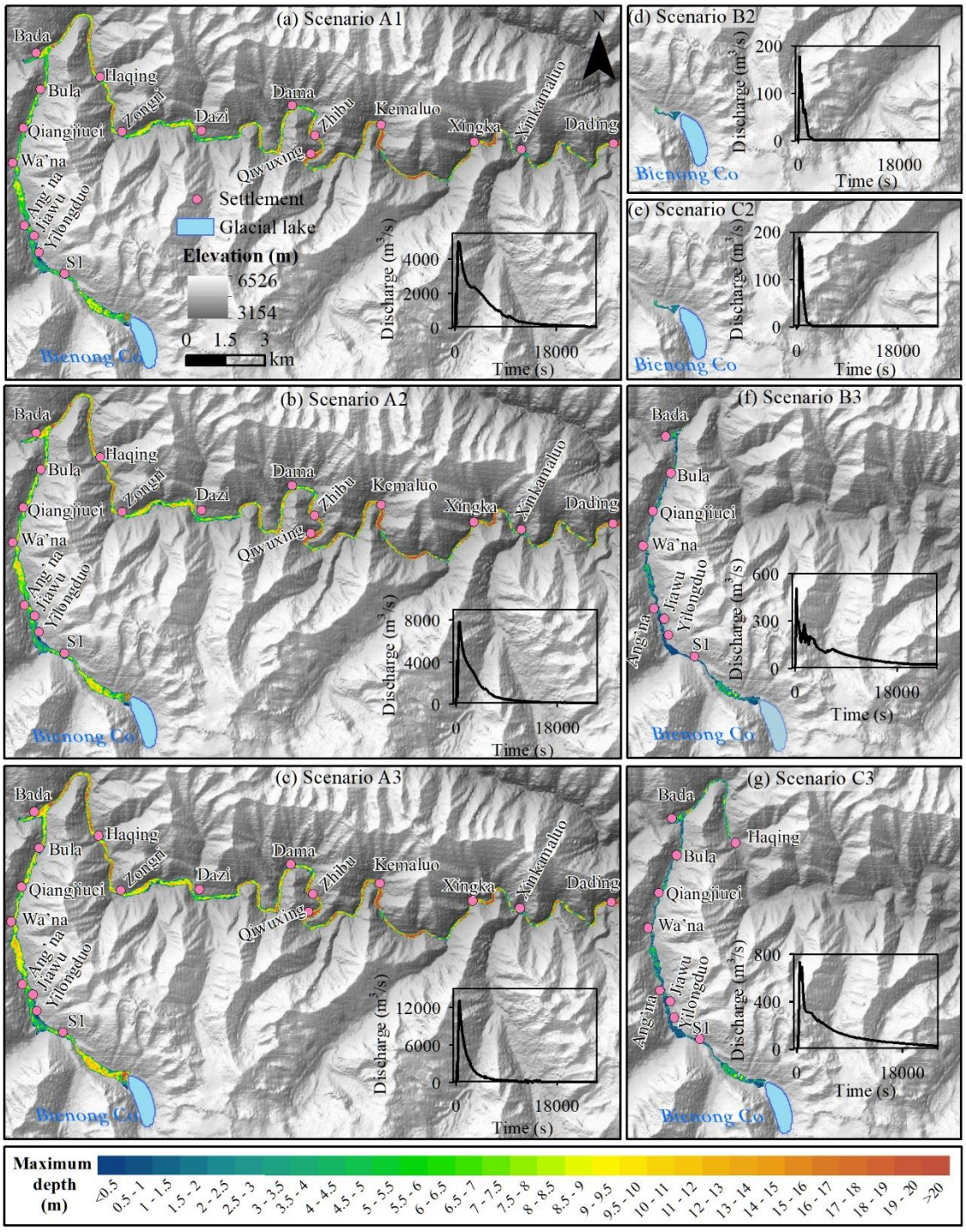

Figure 11. Propagation of flood water downstream and the time series of discharge at the breach outlet (inset) for different scenarios.

GLOFs of different magnitudes pose different potential hazards to each settlement along the flow channel. Scenario A3 produces the most severe threat of GLOF to the downstream region. Six settlements, including Ang'na, Wa'na, Haqing, Kemaluo, Xinka, and Dading, will be completely submerged by flooding. Kemaluo village, located 37.9 km downstream of Bienong Co, will experience the relatively largest maximum flow depth of 19.8 m, and the village of Ang'na, having a distance of 6.0 km from Bienong Co, will experience the relatively smallest maximum flow depth of 6.1 m. Wa'na village is the most affected of all of the villages by GLOF due to the most flooded houses. Eight settlements of S1, Qiangjiuci, Bula, Bada, Dama, Zhibu, Qiwuxing, Xingka, and Xinkamaluo, will be partially flooded. The maximum flow depth of 11.0 m in Bada village is the largest, and that of 7.2 m in both Dama and Zhibu villages is the smallest. Four settlements, Yilongduo, Jiawu, Zongri, and Dazi are spared from floods, in which Yilongduo may be slightly affected, while Dazi is the safest village

due to its far distance from the river. Flooding in Scenario A2 has a relatively small impact on downstream villages compared to that of Scenario A3, showing the reduced extent of inundation and flow depth. Ang'na and Haqing villages have reduced flood ranges. However, villages Wa'na, Kemaluo, Xinka, and Dading will still be completely flooded, but the maximum flow depth is reduced from 16.5 m, 19.8 m, 12.5 m, and 17.5 m, to 13.6 m, 19.3 m, 12.0 m, and 16.6 m, respectively. For the nine villages that are partially affected by Scenario A2, they are still affected by flooding of Scenario A2 except for Dama village, but the impact of flooding is diminished. Scenario A1 differs from Scenario A3 in that Dama and Xingkamaluo villages were spared from flooding, while other villages experienced significant reductions in flood extent and inundation depth. The floods of Scenarios B3 and C3 have significantly less impact in the downstream than the above three scenarios. Only Wa'na, Qiangjiuci, and Bula villages will be partially affected, with the maximum flow depth of 3.1 m, 1.9 m, and 2.0 m in Scenario B3 and 4.0 m, 2.4 m, and 2.7 m in Scenario C3, respectively (Fig. 12). The total areas of houses, courtyards, and farmlands (around settlement) affected by Scenarios A1, A2, A3, B3, and C3 were estimated to be 23,984 m^2, 32,076 m^2, 41,038 m^2, 3,820 m^2, and 3,918 m^2, respectively. In Scenarios A1, A2, A3, all 13 bridges and road with a length of approximately 35 km are within the flood zones, and in Scenarios B3 and C3, there are four bridges as well as road with a length of approximately 3.6 km and 6.7 km within the flood zones. Here we only assess the potential impact of floods on these man-made structures, but the concrete magnitude of the impact is beyond the scope of this study.

The peak discharge and velocity of GLOFs in these villages experience a gradually decreasing process, while the arrival time of peak discharges is prolonged, favoring the evacuation of residents in the downstream area. Peak discharges in S1, Yilongduo, Jiawu, and Ang'na villages, are similar for each scenario, ~4,000 m^3/s of Scenario A1, ~6,000 m^3/s of Scenario A2, and ~10,000 m^3/s of Scenario A3. Wa'na, Qiangjiuci, and Bula villages have similar peak discharges, which are ~3,800 m^3/s, ~5,000 m^3/s, and ~8,000 m^3/s for Scenarios A1, A2, and A3, respectively. Beginning with Bula village, peak discharges of each scenario decrease significantly towards the downstream. Taking Scenario A3 as an example, at Bula village, peak discharge is 7,512 m^3/s, at Haqing village, it becomes smaller than 6,000 m^3/s, at Dama village, it drops below 4,000 m^3/s, at Qiwuxing village it drops below 3,000 m^3/s, and at Xinka village it decreases to below 1,000 m^3/s (Fig. 13). The flood flow velocity varies dramatically, with Scenarios A1, A2, and A3 corresponding to maximum velocities of 8.9 m/s, 12.2 m/s, and 14.9 m/s, respectively, at village S1. At Dading village, the maximum flow velocity of GLOFs is approximately 2m/s.

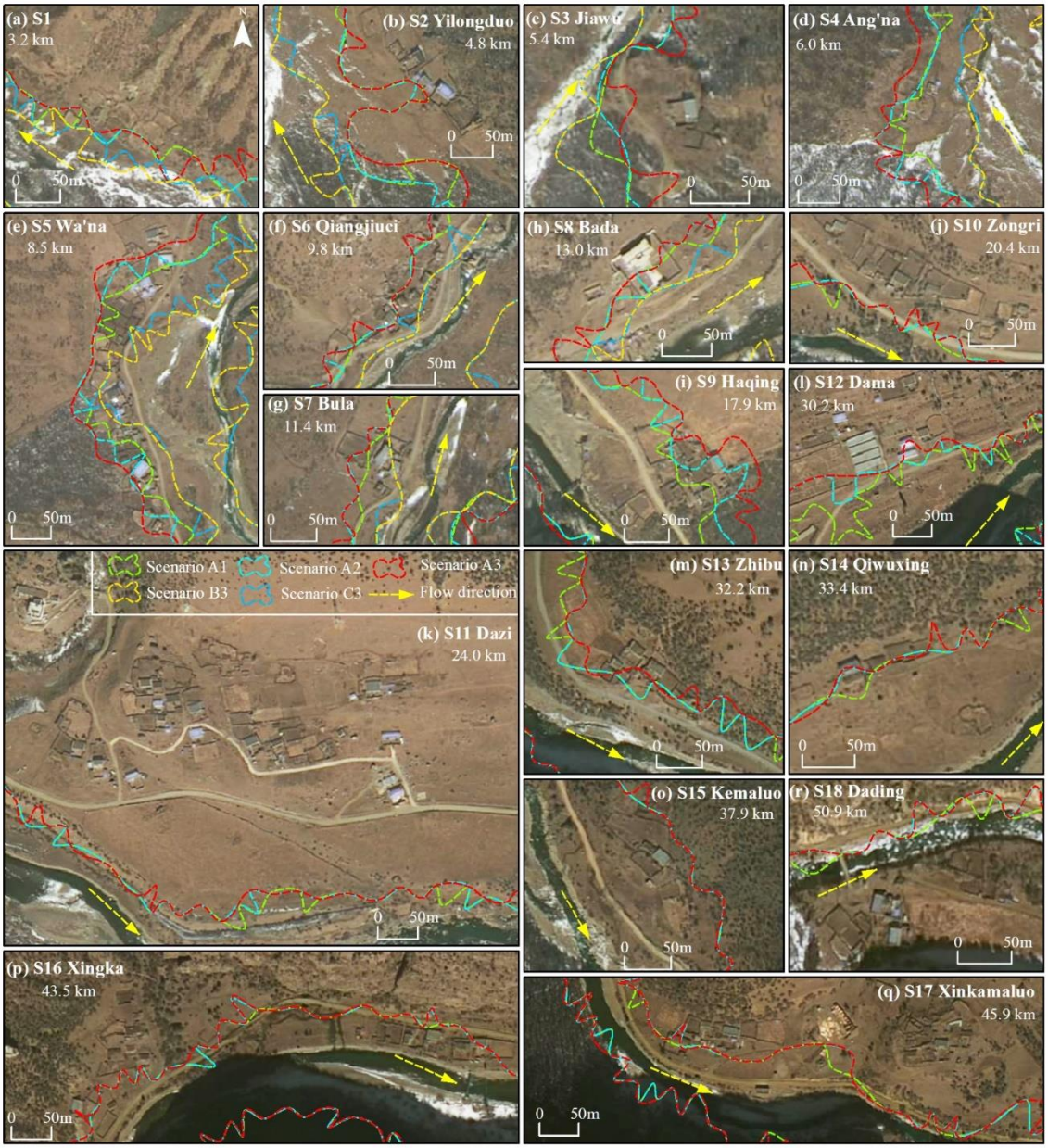

Figure 12. The potential threat of GLOFs to settlements and roads downstream under different ice avalanche and landslide scenarios (the background is the MapWorld image).

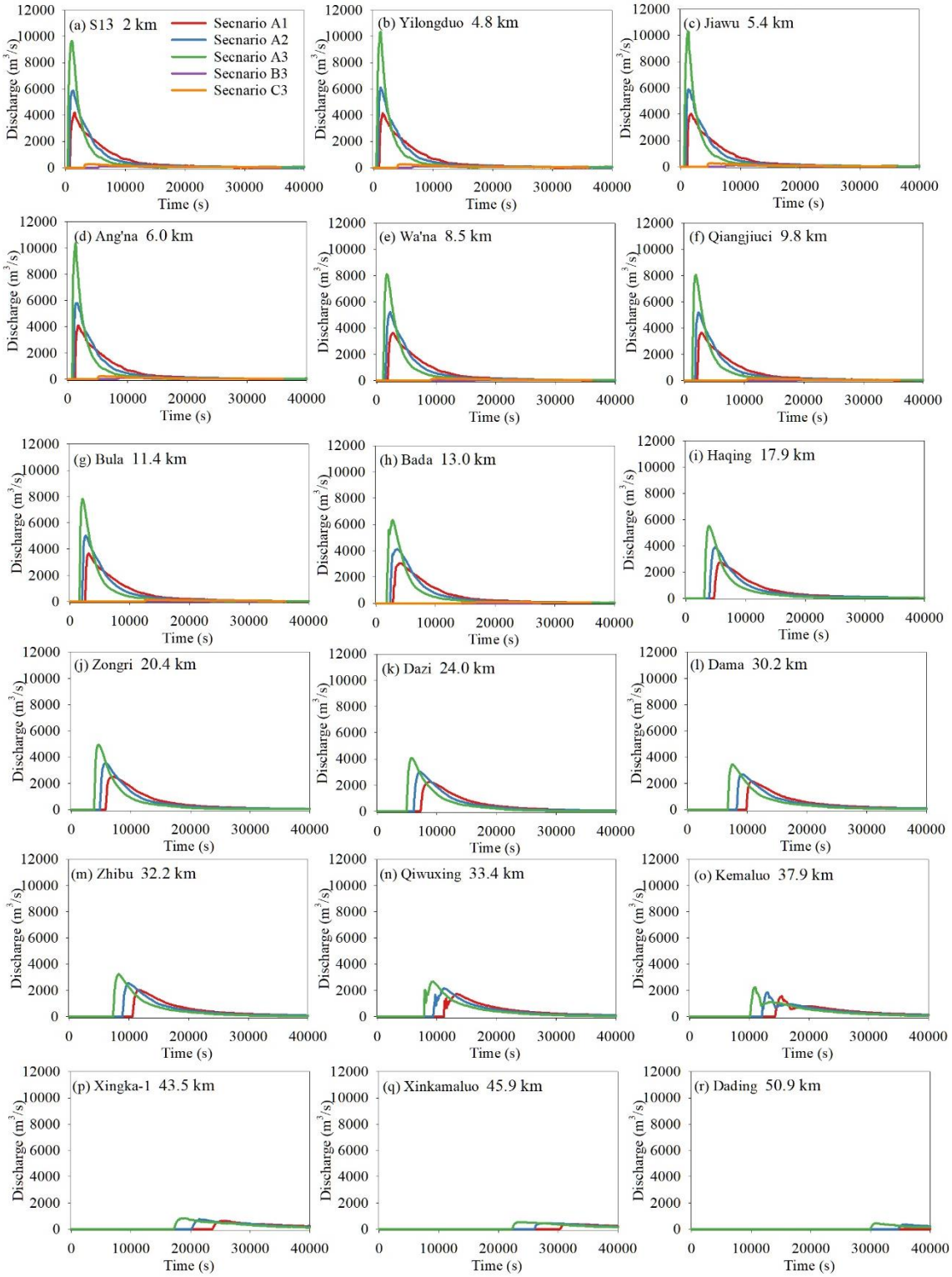

Figure 13. Time series of discharge at different settlements along the flow channel (locations in Fig. 1) of different scenarios.

495

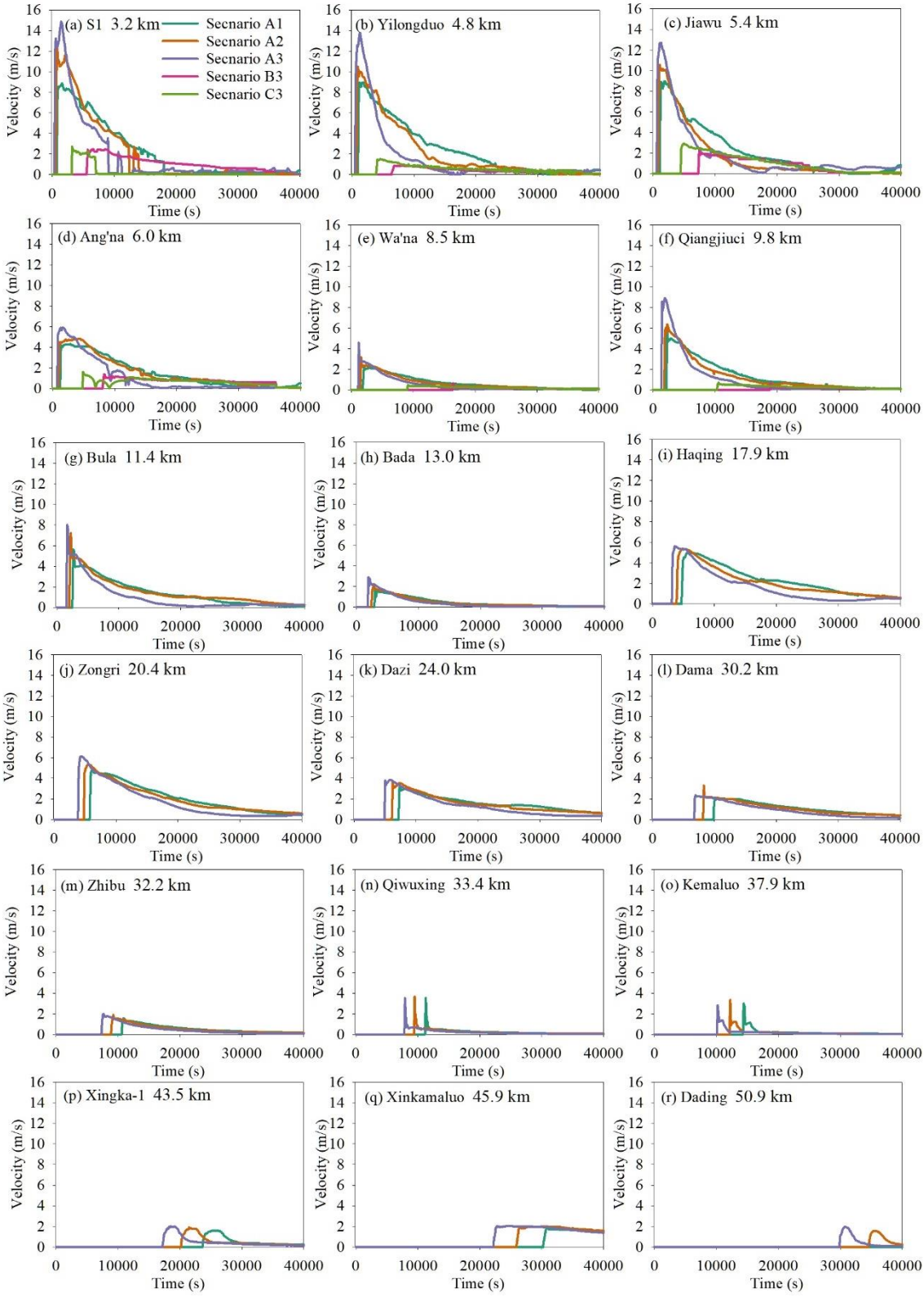

Figure 14. Time series of velocity at different settlements along the flow channel (locations in Fig.1) of different scenarios.

5 Discussion

5.1 Lake volume of Bienong Co

Based on the accurate bathymetric results of the USV, we found that the maximum and depth average of Bienong Co were 181 m and 85.4 m, respectively, with the lake volume of 102.3 × 10^6 m^3 in August 2020. Considering the rarity of bathymetric data but the frequent occurrence of GLOFs in the region, we attempted to obtain more information about glacial lakes in the region by using bathymetry and lake volume of Bienong Co. First, relationships with significant correlations for area-volume, area-depth, and depth-volume of Bienong Co were established (Fig. 15), and it is hoped that this information could provide a valuable data reference for future studies of Bienong Co and other glacial lakes in the region. Then, we compared the depth and lake volume information of Bienong Co with other glacial lakes that have been measured. At present, there are few glacial lakes with measured bathymetry on the Tibetan Plateau, and they are mainly concentrated in the Himalayas of Nepal and the Poiqu Basin of Tibet, China. Longbasaba is an end moraine-dammed glacial lake located at the northern slope of the Himalayas, which had an area of 1.22 ± 0.02 km^2 in 2009, with average and maximum depths of 48 ± 2 m and 102 ± 2 m, respectively, and a volume of 64 × 10^6 m^3 (Yao et al., 2012). Although the area of Longbasaba is approximately 6% larger than that of Bienong Co, the lake volume is only 60% of that of Bienong Co. This example shows that a glacial lake in the temperate glaciation zone is significantly larger in volume than a similarly-sized glacial lake in the continental glaciation zone. However, due to the lack of measured bathymetric data of glacial lakes in the continental glaciation zone, no more comparisons can be made. We compared the depth and lake volume of Bienong Co with other glacial lakes in the temperate glaciation zone. The area of Lugge glacial lake in Butan was approximately 1.17 km^2 in 2004, which is slightly larger than that of Bienong Co, but its average depth and maximum depth were 49.8 m and 126 m, respectively, with a lake volume of 58×10^6 m^3 (Yamada, 2004), which was smaller than the corresponding value of Bienong Co. At the time of bathymetry, both South Lhonak lake in India and Imja glacial lake in Nepal had an area of approximately 1.3 km^2, which is approximately 13% larger than that of Bienong Co, but both lakes have 64% and 76% of Bienong Co's volume, respectively (Sharma et al., 2018; Haritashya et al., 2018). Areas of Raphsthren glacial lake in Buhtan and Tsho Rolpa glacial lake in Nepal were 1.4 km^2 and 1.5 km^2 when bathymetries were carried out, which are 22% and 30% larger than that of Bienong Co, but their lake volume is 65% and 84% of that of Bienong Co, respectively (Geological Survey of India, 1995; ICIMOD, 2011). The area of Lower Barun glacial lake in Nepal was 1.8 km^2, which is 57% larger than that of Bienong Co, but the lake volume was 112×10^6 m^3, which is only 9% larger than that of Bienong Co (Haritashya et al., 2018), showing that Bienong Co is relatively deeper and has larger volume.

Additionally, due to the scarcity of glacial lake bathymetry data and their importance for GLOF hazards, scholars have proposed relationships to estimate volumes of glacial lakes through area, width, and length (O'Connor et al., 2001; Huggel et al., 2002; Sakai, 2012; Wang et al., 2012a; Yao er al., 2012, Cook and Quincey, 2015; Qi et al., 2022). We estimate the lake volume of Bienong Co using published equations based on glacial lakes on the Tibetan Plateau, and the results show that the eight published volume-area/width-length relationships all underestimate the volume of Bienong Co to varying degrees. It can be inferred that Bienong Co is the relative deepest glacial lake among these on the Tibetan Plateau that currently have been measured. Whether this is unique to Bienong Co or a common feature of glacial lakes in the region is not yet known, as few glacial lakes in this region have field bathymetry. Future bathymetry is necessary for more typical glacial lakes in the region.

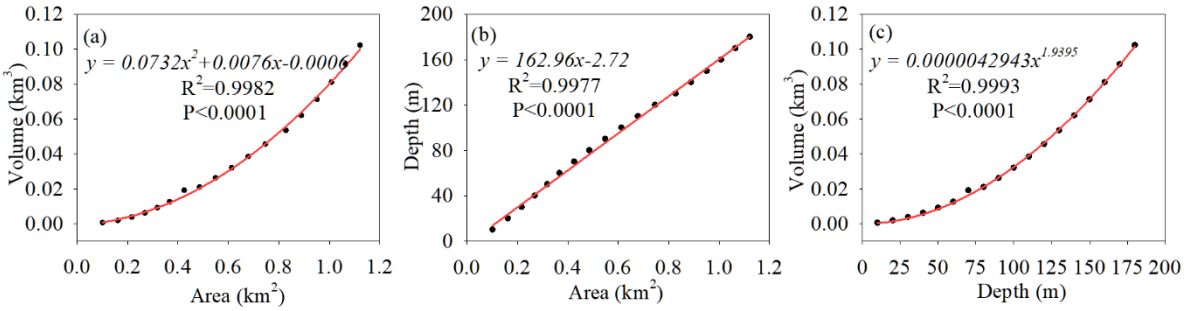

Figure 15. Fitting relationship of (a) area and volume, (b) area and depth and (c) depth and volume of Bienong Co.

Table 1. Calculated volumes of Bienong Co based on published volume-area relationships for glacial lakes in the Tibetan Plateau.

No	Source		Relationships	Calculated Volume	Error (%)
1	Qi et al., (2022)	(1)	$V=0.04066A^{1.184}-0.003207w_{mx}/l_{mx}$	46.9×10^6 m^3	-54%
2		(2)	$V=0.0126A^2+0.0056A+0.0132$	36.3×10^6 m^3	-65%
3	Wang et al., (2012)		$V=0.0354A^{1.3724}$	42.9×10^6 m^3	-58%
4	Sakai (2012)		$V=0.04324A^{1.5307}$	53.6×10^6 m^3	-48%
5	Yao et al., (2012)		$V=0.0493A^{0.9304}$	56.1×10^6 m^3	-45%
6	Fujita et al., (2013)		$V = 0.055A^{1.25}$	65.5×10^6 m^3	-36%
7	Khanal et al., (2015)		$V = 0.0578A^{1.5}$	71.3×10^6 m^3	-30%
8	Zhou et al., (2020)		$V=0.0717\ w_{mx}{}^2l_{mx}$	70.3×10^6 m^3	-31%

Note: Error = (volume of empirical formulas – bathymetrically-derived volume) / bathymetrically-derived volume × 100%.

5.2 Modelling explanation

Triggers are the beginning of the simulated GLOFs process chain in this study, and we only consider ice avalanche and landslide scenarios, instead of other factors, such as increased glacial meltwater and heavy precipitation. The magnitude, location, and probability of ice avalanches and landslides constitute the largest sources of uncertainty in this study. Ice avalanches are the trigger for over 70% of GLOFs on the Tibetan Plateau, but there is no reliable reference for the magnitude, including the release area and depth, of previous ice avalanche events. Ice avalanches in this study come from the mother glacier tongue, where the slope is relatively steep and the fissures are well-developed. We simulated three different-magnitude ice avalanches, and each scenario assumes that the ice body breaks off in the vertical direction until it reaches the lake surface, which is unrealistic and may overestimate the volume of the ice avalanche. The RAMMS model can estimate the possible release volume based on the input DEM data and the release area, as well as the release depth, with the estimated released volume of 5×10^6 m^3, 13.1×10^6 m^3, and 41.3×10^6 m^3 for Scenarios A1, A2, and A3, respectively. However, simulations show that approximately 76% (3.8×10^6 m^3), 37% (4.9×10^6 m^3), and 14% (5.8×10^6 m^3) of the estimated release volume enter the lake in Scenarios A1, A2, and A3, respectively. The simulation duration is set to 600 s to ensure integrity of the ice avalanche process, and most of the ice avalanche has already entered the lake within 100 s. The difference between the volume of the ice avalanche entering the lake and the estimated release volume is mainly determined by the slope between the ice body and the lake and the distance from the lake. The gentler slope and far distance from the lake of the ice body in Scenarios A2 and A3 result in fewer ice avalanches entering the glacial lake, and affect the process of ice avalanche material entering the lake, e.g., Scenarios A2 and A3 have stronger fluctuations in the ice avalanche process than Scenario A1. In addition, we also consider landslides as a trigger given the failure of Jinwu Co in 2020. Two release areas were selected by referring to the slope and location of Jinwu Co's landslide. However, the release depth has no

quantified reference data and we assumed three release depths of 2 m, 5 m, and 10 m for each release area to simulate the consequences resulting from as many scenarios as possible.

A reliable simulation of potential disaster events such as ice avalanche or landslide in the future using scientific methods can assist people understand the possible risks and raise prevention awareness. However, accurate prediction is generally difficult due to limited geological information and details of triggering mechanisms such as extreme rainfall event. In this study, the RAMMS model was used to estimate the consequences of potential ice avalanche and landslide events. The accuracy and resolution of DEM data is crucial for this model calculations, which can greatly affect the topography and the avalanche and landslide pathways, and is concerned with the accurate reflection of the process of an ice avalanche event (Schneider et al., 2010). The issue of DEM accuracy in glacial environments is mainly due to the topographic changes between the times of DEM acquisition and the avalanche event. The DEM with lower resolution can lead to an overestimation of sediment area and an underestimation of sediment thickness (Cesca and D'Agostino, 2008). The ALOS PALSAR DEM product used in this study was released globally in October 2014, with a spatial resolution of 12.5 m, which can generally reflect the intensity and pathway of the ice avalanche and landslide events simulated in this study. The volumes of future ice avalanches or landslides will almost certainly be smaller than the volumes formulated in this study due to glacier melting caused by climate warming. Moreover, the dry-Coulomb type friction μ and the viscous-turbulent friction ξ can also influence on the modelling results (Bezak et al., 2019). Mikoš and Bezak (2021) suggested that the ice avalanche or landslide magnitude slightly decreases and increases with increasing friction parameters μ and ξ, while the correlation is not strong. Schneider et al. (2014) found that higher μ and ξ combinations lead to higher peak velocities, faster stopping mechanisms, and hence shorter process durations. The value of μ and ξ covered wide ranges in the past applications (Mikoš and Bezak, 2021), and they were usually calibrated by actual events. We chose 0.12 and 1,000 m s^{-2} as the values of μ and ξ in this study, which were used in the avalanche simulation of Lake 513 (Schneider et al., 2014).

The BASEMENT model was applied to simulate the subsequent chains of GLOF process following ice avalanches and landslides. Much of the work on the generation, propagation and run-up of impulse wave has been focused on empirical models that replicate wave characteristics based on laboratory observations (Heller and Hager, 2010). Numerical simulations have been limited to simplified 2D SWE simulations (Ghozlani et al., 2013), however, the 2D SWE is not adequate to simulate waves generated by avalanches because of the large energy dissipation due to significant vertical accelerations (Lala et al., 2018). Therefore, empirical models are often used to calibrate the numerical simulations, such as the Heller-Hager model was employed to calibrate the simulation of the BASEMENT model in past studies (Byers et al., 2018; Lala et al., 2018). Nevertheless, the numerous parameters required by the Heller-Hager model are still subject to potential uncertainties owing to its simple quantifications about the geometry of the lake. It is also mentioning that lake hydrodynamic model can only accept inflow in the form of water volume, but not the material itself inflow, such as moraine material, ice, snow, and their combinations (Kafle et al., 2016). Generally, simulations are calibrated by controlling the height and depth of the release area and converting the density between the material and water to influence the flow height and flow velocity in the model as avalanches enter a lake. However, the energy dissipation between the water and the true avalanche mixture is different, and the model can't present the real situation of the avalanche fluid mixing with a lake (Somos-Valenzuela et al., 2016). Furthermore, the maximum area of TIN representing a lake also has influence on the wave amplitude, smaller areas lead to finer values, which have little influence on the absolute value of wave amplitude. The grain size distribution of Bienong Co's dam is an important parameter in simulating the moraine dam's erosions, but it is not obtained in this study. The simulations were performed by referencing an inventory of glacial lakes in the Indian Himalayas that have been validated as generally reliable (Worni et al., 2013), but errors in Bienong Co are inevitable.

The ALOS PALSAR DEM with a spatial resolution of 12.5 m has been widely used in studies on cryospheric changes and disasters. It was pre-processed to fill sinks in this study, but there is still the phenomenon of flood water accumulating in deep puddles, especially in the relatively narrow valley. We manually smoothed several large bumps according to the

elevation of the upstream and downstream. However, there are still some smaller bumps that converge the flow to a section of the flow channel, mainly in the downstream area. Therefore, the flooding situation in Qiwuxing, Kemaluo, Xingka and Dading villages might be overestimated, especially in the former two villages because they are relatively far away from the river. The latter two villages are still very likely to be threatened by flooding due to their proximity to the river. The resolution of the ALOS PALSAR DEM is clearly insufficient for accurate simulation of flooding in the river-channel. Therefore, more precise topographic information, such as DEM data generated from panchromatic stereo images with spatial resolutions better than 0.8 m obtained by the Gaofen-7 satellite and UAV-derived DEM products with low-cost are prospective. The frictional resistance within the downstream channel of Bienong Co is derived from the GLC10 LULC data, which basically fits the reality and has litter error of the simulations. GLOF flow processes can be very complex (Zhou et al., 2019), and flows can transform from clear water flow to hyperconcentrated flow and then to debris flow, and these rheological transformations can occur in both space and time as the flow evolves (Worni et al., 2014). In this study, we do not consider the effects of sediment on flow rheology, as well as the erosion and deposition of sediment along the flow path.

Emmer et al. (2022) divided the research evolution of GLOF process chains simulations into three stages, and this study belongs to the second stage, i.e., applying tailored physically based simulation tools for each component of the process chain and coupling them at the process boundaries. The third stage is the two-phase (Pudasaini, 2012) and three-phase (Pudasaini and Mergili, 2019) mass flow models and related simulation tools (Mergili et al., 2017; Mergili and Pudasaini, 2021) and the integrated simulations of the entire GLOF process chain in one single simulation step. The main advantage of the methods in the second stage is the simplicity and operability, with the convenient GUI interface of software in different links. Models for different links have been matured and widely applied in the corresponding fields with reliable performance and accessibility of the required parameters. However, the third stage is undoubtedly the focus of future research to investigate the whole GLOF flooding process with more detail, in-depth, and better to reduce uncertainty in the coupling between different models. This will certainly involve more detailed parameters, increasing the difficulty of the simulation.

6 Conclusion

As a moraine-dammed glacial lake located in a temperate glaciation region, Bienong Co has been highly regarded by local government due to its larger area and high potential for GLOF hazards. Based on bathymetric data, remote sensing images and DEM data, combined with the multiple models of RAMMS, BASEMENT, and Heller-Hager, we completed a comprehensive investigation of the potential GLOF process chain of Bienong Co, including the initial mass movement from the mother glacier and the lateral moraine slope, displacement wave generation and propagation in the lake, overtopping flow and erosion on the moraine dam, and subsequent downstream flooding. The following main results were obtained:

(1) According to the field bathymetric data, the lake basin morphology of Bienong Co features a relatively flat basin bottom and steep flanks, with the slope near the glacier (16.5˚) being steeper than that near the moraine dam (11.3˚). The water storage of Bienong Co was ~102.3 × 10^6 m^3 in August 2020, with a maximum depth of ~181 m. The enormous water storage combined with the fissure-developed mother glacier tongue, steep lateral moraine slope, steep distal facing slope of the moraine dam, and low freeboard make it possess high GLOF potential.

(2) The volume of materials entering the lake for the three scenarios of ice avalanches (A1, A2, and A3) is much larger than that of the six scenarios of landslides (B1, B2, and B3 and C1, C2, and C3). Volumes of ice avalanches entering the lake in Scenarios A1, A2, and A3 are 3.8 × 10^6 m^3, 4.9 × 10^6 m^3, and 5.8 × 10^6 m^3, respectively. Among the six landslide scenarios, Scenario B1 releases a minimum volume of 0.03 × 10^6 m^3 and Scenario C3 releases a maximum volume of 0.30×10^6 m^3. As a result, the impact zone, maximum flow height, and maximum flow velocity in the lake also show that Scenarios A1, A2, and A3 are significantly larger than the other six scenarios, in which Scenario B1 is the smallest and Scenario A3 is the largest. Wave amplitudes near the moraine dam in Scenarios A1, A2, and A3 are 17.1 m, 20.2 m, and

25.2 m, respectively. The overtopping flow of all three scenarios causes erosion of the dam, with little difference in breach depth (19.0 m, 19.1 m, and 19.3 m), but large difference in breach width (295.0 m, 339.4 m, and 368.5 m). The volumes of water lost in the lake of the three scenarios are 24.1 × 10^6 m^3, 25.3 × 10^6 m^3, and 26.4 × 10^6 m^3, and the flood peak flows are 4,996 m^3/s, 7,817 m^3/s, and 13,078 m^3/s, respectively. Among the other six scenarios, only Scenarios B3 and C3 with larger magnitudes formed breaches on the moraine dam, with breaches of 6.5 m and 7.9 m in depth and 153 m and 169 m in width, respectively.

(3) Floods all pass through 18 settlements in the downstream river in 20 h, with inundation areas of 7.6 km^2, 8.0 km^2, and 8.5 km^2, as well as average water depths of 8.4 m, 9.1 m, and 10.0 m, respectively. The GLOFs threatened more than half of the villages in the downstream region. Scenarios B1 and B2 and C1 and C2 produce very limited overtopping flow that cannot pose a threat to the downstream region. Both Scenarios B3 and C3 produced floods that flow through eight downstream settlements within 20 h and had a relatively small impact on them.

(4) Bienong Co is the relative deepest glacial lake among those on the Tibetan Plateau that have currently been measured and is markedly different from glacial lakes on the south slope of the Himalayas. Furthermore, it is also important to use high-precision topographic data for disaster simulation of GLOF lakes.

Code and data availability. The Landsat MSS/TM/OLI image are available from the United States Geological Survey (https://earthexplorer.usgs.gov/). The AST14DEM dataset and ALOS PALSAR DEM used in this study can be obtained from the National Aeronautics and Space Administration (NASA) EARTHDATA website (https://earthdata.nasa.gov/). The MapWorld image is provided by the National Platform for Common Geospatial Information Services (https://www.tianditu.gov.cn/). The GLC10 LULC product is available from http://data.ess.tsinghua.edu.cn/fromglc10_2017v01.html.

Author contributions. HD contributed the conceptualization, methodology, software, formal analysis, visualization and writing of the original draft; XY contributed the conceptualization, supervision, funding acquisition, investigation of the glacial lake, as well as review and editing of the manuscript; YZ, HJ, and QW contributed the investigation of the glacial lake; ZD, BW and QW contributed the model progress; JH contributed the setting up the experimental equipment and obtaining data.

Competing interests. The authors declare that they have no conflict of interest.

Financial support. This research has been supported by the National Key Research Program of China (grant no. 2019YFE0127700), the National Natural Science Foundation of China (grant nos. 41861013 and 42071089), "Innovation Star" of the Outstanding Graduate Student Program in Gansu Province (grant no. 2021-CXZX-215), Northwest Normal University's 2020 Graduate Research Grant Program (grant no. 2020KYZZ001012), and the Outstanding PhD Student Program in Gansu Province (no. 22JR5RA139).

References

Bartelt, P., Buehler, Y., Christen, M., Deubelbeiss, Y., Graf, C., McArdell, B., Sals, M., and Schneider, M.: RAMMS: Rapid mass movement simulation: a numerical model for debris flows in research and practice, User Manual v1.5 - Debris Flow, Swiss Institute for Snow and Avalanche Research SLF, Birmensdorf, 2013.

Bezak, N., Sodnik, J., and Mikoˇs, M.: Impact of a random sequence of Debris flows on torrential fan formation, Geosciences, 9, 64, https://doi.org/10.3390/geosciences9020064, 2019.

Bolch, T., Peters, J., Yegorov, A., Pradhan, B., Buchroithner, M., and Blagoveshchensky, V.: Identification of potentially

dangerous glacial lakes in the northern Tien Shan, Nat. Hazards, 59, 3, 1691–1714, https://doi.org/10.1007/s11069-011-9860-2, 2011.

Byers, A. C., Rounce, D. R., and Shugar, D. H.: A rockfall-induced glacial lake outburst flood, Upper Barun Valley, Nepal, Landslides, 16, 533–549, https://doi.org/10.1007/s10346-018-1079-916, 2018.

Byers, A. C., Chand, M. B., and Lala, J.: Reconstructing the history of glacial lake outburst floods (GLOF) in the Kanchenjunga conservation area, east Nepal: an interdisciplinary approach, Sustainability, 12, 5407, https://doi.org/10.3390/su12135407, 2020.

Brun, F., Berthier, E., Wagnon, P., Kääb, A., and Treichler, D.: A spatially resolved estimate of High Mountain Asia glacier mass balances from 2000 to 2016, Nat. Geosci., 10, 668–673, https://doi.org/10.1038/ngeo2999, 2017.

Carrivick, J. L. and Tweed, F. S.: A global assessment of the societal impacts of glacier outburst floods, Global. Planet. Change., 144, 1–16, https://doi.org/10.1016/j.gloplacha.2016.07.001, 2016.

Cesca, M. and D'Agostino, V.: Comparison between FLO-2D and RAMMS in debris-flow modelling: a case study in the Dolomites, WIT Trans. Eng. Sci., 60, 197–206, https://doi.org/10.2495/DEB080201, 2008.

Cheng, Z. L., Zhu, P., Dang, C., and Liu, J. J.: Hazards of debris flow due to glacier lake outburst in Southeastern Tibet, Journal of Glaciology and Geocryology, 30, 954–959, https://doi.org/CNKI:SUN:BCDT.0.2008-06-006, 2008.

Cheng, Z. L., Liu, J. J., and Liu, J. K.: Debris flow induced by glacial-lake break in Southeast Tibet, Earth Science Frontiers, 16, 207–214, https://doi.org/10.2495/DEB100091, 2009.

Christen, M., Kowalski, J., and Bartelt, P.: RAMMS: numerical simulation of dense snow avalanches in three-dimensional terrain, Cold Reg. Sci. Technol., 63, 1–14, https://doi.org/10.1016/j.coldregions.2010.04.005, 2010.

Cook, S. J. and Quincey, D. J.: Estimating the volume of Alpine glacial lakes, Earth. Surf. Dynam., 3, 559–575, https://doi.org/10.5194/esurf-3-559-2015, 2015.

Cook, K. L., Andermann, C., Gimbert, F., Adhikari, B. R., and Hovius, N.: Glacial lake outburst floods as drivers of fluvial erosion in the Himalaya, Science, 362, 53–57, https://doi.org/10.1126/ science.aat 4981, 2018.

Coon, W. F.: Estimation of roughness coefficients for natural stream channels with vegetated banks, United States Geological Survey water-supply paper, 2441, 1998.

Cui, P., Ma, D. T., and Chen, N. S.: The initiation, motion and mitigation of debris flow caused by glacial lake outburst, Quaternary Sciences, 23, 621–628, https://doi.org/10.1016/S0955-2219(02)00073-0, 2003.

Dehecq, A., Gourmelen, N., Gardner, A. S., Brun, F., Goldberg, D., Nienow, P. W., Berthier, E., Vincent, C., Wagnon, P., and Trouvé, E.: Twenty-first century glacier slowdown driven by mass loss in High Mountain Asia, Nat. Geosci., 12, 22–27, https://doi.org/10.1038/s41561-018-0271-9, 2019.

Duan, H. Y., Yao, X. J., Zhang, D. H., Qi, M. M., and Liu, J.: Glacial lake changes and identification of potentially dangerous glacial lakes in the Yi'ong Zangbo River Basin, Water-Sui, 12, 538, https://doi.org/10.3390/w12020538, 2020.

Emmer, A. and Cochachin, A.: The causes and mechanisms of moraine-dammed lake failures in the Cordillera Blanca, North American Cordillera and Himalaya, AUC. Geogr., 48, 5–15, https://doi.org/10.14712/23361980.2014.23, 2013.

Emmer, A. and Vilímek, V.: New method for assessing the susceptibility of glacial lakes to outburst floods in the Cordillera Blanca, Peru, Hydrol. Earth Syst. Sci., 18, 3461–3479, https://doi.org/10.5194/hess-18-3461-2014, 2014.

Emmer, A., Allen, S. K., Carey, M., Frey, H., Huggel, C., Korup, O., Mergili, M., Sattar, A., Veh, G., Chen, T. Y., Cook, S. J., Correas-Gonzalez, M., Das, S., Diaz Moreno, A., Drenkhan, F., Fischer, M., Immerzeel, W. W., Izagirre, E., Joshi, R. C., Kougkoulos, I., Knapp, R. K., Li, D. F., Majeed, U., Matti, S., Moulton, H., Nick, F., Piroton, V., Rashid, I., Reza, M., Figueiredo, A. R., Riveros, C., Shrestha, F., Shrestha, M., Steiner, J., Walker-Crawford, N., L. Wood, J., and Yde, J. C.: Progress and challenges in glacial lake outburst flood research (2017-2021): a research community perspective, Nat. Hazards Earth Syst. Sci., 22, 3041–3061, https://doi.org/10.5194/nhess-22-3041-2022, 2022.

Evans, S. G.: The maximum discharge of outburst floods caused by the breaching of man-made and natural dams, Can.

Geotech. J., 24, 385–387, https://doi.org/10.1139/t87-062, 1987.

Fujita, K., Sakai, A., Takenaka, S., Nuimura, T., Surazakov, A. B., Sawagaki, T., and Yamanokuchi, T.: Potential flood volume of Himalayan glacial lakes, Nat. Hazards Earth Syst. Sci., 13, 1827–1839, https://doi.org/10.5194/nhess-13-1827-2013, 2013.

Geological Survey of India: Geology environmental hazards and remedial measures of the Lunana Area, Gasa Dzongkhang, Report of 1995 Indo-Bhutan Expedition, Bhutan Unit, Geological Survey of India, Samtse, 1995.

Ghozlani, B., Zouhaier, H., and Khlifa, M.: Numerical study of sur- face water waves generated by mass movement, Fluid Dyn. Res., 45, 055506, https://doi.org/10.1088/0169-5983/45/5/055506, 2013.

Haeberli, W., Kääb, A., Vonder Mühll, D., and Teysseire, P.: Prevention of outburst floods from periglacial lakes at Grubengletscher, Valais, Swiss Alps, J. Glaciol., 47, 111–122, https://doi.org/10.3189/172756501781832575, 2001.

Haritashya, U. K., Kargel, J. S., Shugar, D. H., Leonard, G. J., Strattman, K., Watson, C. S., Shean, D., Harrison, S., Mandli, K. T., and Regmi, D.: Evolution and controls of large glacial lakes in the Nepal Himalaya, Remote Sens-Basel, 10, 798, https://doi.org/10.3390/rs10050798, 2018.

Harrison, S., Kargel, J. S., Huggel, C., Reynolds, J., Shugar, D. H., Betts, R. A., Emmer, A., Glasser, N., Haritashya, U. K., Klimeš, J., and Reinhardt, L.: Climate change and the global pattern of moraine-dammed glacial lake outburst floods, The Cryosphere, 12, 1195–1209, https://doi.org/10.5194/tc-12-1195-2018, 2018.

Heller, V., Hager, W., and Minor, H. E.: Landslide generated im- pulse waves in reservoirs: Basics and computation, Laboratory of Hydraulics, Hydrology, and Glaciology, ETH Zürich, Switzerland, 172, 2009.

Heller, V. and Hager, W. H.: Impulse product parameter in landslide generated impulse waves, J. Waterw. Port. Coast., 136, 145–155, https://doi.org/10.1061/(ASCE)WW.1943-5460.0000037, 2010.

Huang, L., Zhu, L. P., Wang, J. B., Ju, J. T., Wang, Y., Zhang, J. F., and Yang, R. M.: Glacial activity reflected in a continuous lacustrine record since the early Holocene from the proglacial Laigu Lake on the southeastern Tibetan Plateau, Palaeogeogr. Palaeocl., 456, 37–45, https://doi.org/10.1016/j.palaeo.2016.05.019, 2016.

Huggel, C., Kääb, A., Haeberli, W., Teysseire, P., and Paul, F.: Remote sensing based assessment of hazards from glacier lake outbursts: a case study in the Swiss Alps, Can. Geotech. J., 39, 316–330, https://doi.org/10.1139/t01-099, 2002.

Huggel, C., Haeberli, W., Kääb, A., Bieri, D., and Richardson, S.: An assessment procedure for glacial hazards in the Swiss Alps, Can. Geotech. J., 41, 1068–1083, https://doi.org/10.1139/t04-053, 2004.

International Centre for Integrated Mountain Development (ICIMOD): Glacial lakes and glacial lake outburst floods in Nepal, ICIMOD, Kathmandu, 99, 2011.

Kafle, J., Pokhrel, P. R., Khattri, K. B., Kattel, P., Tuladhar, B. M., and Pudasain, S. P.: Landslide-generated tsunami and particle transport in mountain lakes and reservoirs, Ann. Glaciol., 57, 232–244, doi: 10.3189/2016AoG71A034, 2016.

Kääb, A., Berthier, E., Nuth, C., Gardelle, J., and Arnaud, Y.: Contrasting patterns of early twenty-first-century glacier mass change in the Himalayas, Nature, 488, 495–498, https://doi.org/10.1038/nature11324, 2012.

Kääb, A., Treichler, D., Nuth, C., and Berthier, E.: Brief communication: contending estimates of 2003-2008 glacier mass balance over the Pamir-Karakoram-Himalaya, The Cryosphere, 9, 557–564, https://doi.org/10.5194/tc-9-557-2015, 2015.

Ke, C. Q., Kou, C., Ludwig, R., and Qin, X.: Glacier velocity measurements in the eastern Yigong Zangbo basin, Tibet, China, J. Glaciol., 59, 1060–1068, https://doi.org/10.3189/2013jog12j234, 2013.

Ke, C. Q., Han, Y. F., and Kou, C.: Glacier change in the Yigong Zangbu Basin, Tibet, China (1988 to 2010), Dragon 3Mid Term Results, 724, http://articles.adsabs.harvard.edu/pdf/2014ESASP.724E.16K, 2014.

Lala, J. M., Rounce, D. R., and Mckinney, D. C.: Modeling the glacial lake outburst flood process chain in the Nepal Himalaya: Reassessing Imja Tsho's hazard, Hydro. Earth. Syst. Sci., 22, 3721–3737, https://doi.org/10.5194/hess-2017-683, 2018.

Larrazabal, J. M. and Peñas, M. S.: Intelligent rudder control of an unmanned surface vessel, Expert. Syst. Appl., 55, 106–

117, https://doi.org/10.1016/j.eswa.2016.01.057, 2016.

Li, J.J., Zhen, B. X., and Yang, X. J.: Glaciers in Tibet, Science Press, Beijing, 1986.

Li, D., Shangguan D. H., Wang, X.Y., Ding, Y. J., Su, P. C., Liu, R. L., and Wang, M. X.: Expansion and hazard risk assessment of glacial lake Jialong Co in the central Himalayas by using an unmanned surface vessel and remote sensing, Sci. Total. Environ., 784, 147249, https://doi.org/10.1016/j.scitotenv.2021.147249, 2021.

LIGG/WECS/NEA: Report on first expedition to glaciers and glacier lakes in the Pumqu (Arun) and Poiqu (Bhote-Sun Koshi) River Basins, Xizang (Tibet), China, Sino-Nepalese Joint Investigation of Glacier Lake Outburst Flood in Himalayas in 1987, 192, 1988.

Liu, J. K., Zhou, L. X., Zhang, J. J., and Zhao, W. Y.: Characteristics of Jiwencuo GLOF, Lhari county, Tibet, Geological Review, 67: 17–18. https://doi.org/10.16509/j.georeview.2021.s1.007, 2021.

Liu, S. Y., Pu, J. C., and Deng, X. F.: Glaciers and glacier landscapes in China, Shanghai Popular Science Press, Shanghai, 38–41, 2014.

Liu, W. M., Lai, Z. P., Hu, K. H., Ge, Y. G, Cui, P., Zhang, X. G., and Liu, F.: Age and extent of a giant glacial-dammed lake at Yarlung Tsangpo gorge in the Tibetan Plateau, Geomorphology, 246, 370–376, https://doi.org/10.1016/j.geomorph.2015.06.034, 2015.

Liu, Z. X., Zhang, Y. M., Yu, X., and Yuan, C.: Unmanned surface vehicles: an overview of developments and challenges, Annu. Rev. Control., 41, 71–39, https://doi.org/10.1016/j. arcontrol.2016.04.018, 2016.

Liu, J. k., Zhang, J. J., Gao, Bo., Li, Y. L., Li, M. Y., Wujin, D. J., and Zhou, L. X.: An overview of glacial lake outburst flood in Tibet, China, Journal of Glaciology and Geocryology, 41, 1335–1347, https://doi.org/10.7522/j.issn.1000-0240.2019.0073, 2019.

Lliboutry, L.: Glaciological problems set by the control of dangerous lakes in Cordillera Blanca, Peru, II. Movement of a covered glacier embedded within a rock glacier, J. Glaciol., 18, 255–274, https://doi.org/10.3189/S0022143000021341, 1977.

Lv, R. R., Tang, X. B., and Li, D. J.: Glacial lake outburst mudslide in Tibet, Chengdu University of Science and Technology Press, Chengdu, 69–105, 1999.

Mckillop, R. J. and Clague, J.: Statistical, remote sensing-based approach for estimating the probability of catastrophic drainage from moraine-dammed lakes in southwestern British Columbia, Global Planet Change, 56, 153–171, https://doi.org/10.1016/J.GLOPLACHA.2006.07.004, 2007.

Mergili, M. and Schneider, J. F.: Regional-scale analysis of lake outburst hazards in the southwestern Pamir, Tajikistan, based on remote sensing and GIS, Nat. Hazards Earth Syst. Sci., 11, 1447–1462, https://doi.org/10.5194/nhess-11-1447-2011, 2011.

Mergili, M., Fischer, J. T., Krenn, J., and Pudasaini, S. P.: r.avaflow v1, an advanced open-source computational framework for the propagation and interaction of two-phase mass flows, Geosci. Model Dev., 10, 553–569, https://doi.org/10.5194/gmd-10-553-2017, 2017.

Mergili, M. and Pudasaini, S. P.: r.avaflow-The open source mass flow simulation model, https://www.avaflow.org/, last access: 1 October 2021.

Mikoš, M. and Bezak, N.: Debris flow modelling using RAMMS model in the Alpine environment with focus on the model parameters and main characteristics, Front. Earth Sci. 8:605061. https://doi.org/10.3389/feart.2020.605061, 2021.

Mool, P. K., Bajracharya, S. R., and Joshi, S. P.: Inventory of glaciers, glacial lakes and glacial lake outburst floods, monitoring and early warning systems in the Hindu Kush- Himalayan region: Nepal, ICIMOD & UNEP RRC-AP, 363, 2001.

Neckel, N., Kropáček, J., Bolch, T., and Hochschild, V.: Glacier mass changes on the Tibetan Plateau 2003-2009 derived from ICESat laser altimetry measurements, Environ. Res. Lett., 9, 468–475, https://doi.org/10.1088/1748-9326/9/1/014009, 2014.

Nie, Y., Liu, Q., Wang, J. D., Zhang, Y. L., Sheng, Y. W., and Liu, S. Y.: An inventory of historical glacial lake outburst

floods in the Himalayas based on remote sensing observations and geo-morphological analysis, Geomorphology, 308, 91–106, https://doi.org/10.1016/j. geomorph.2018.02.002, 2018.

O'Connor, J. E., Hardison, J. H., and Costa, J. E.: Debris flows from failures of neoglacial-age moraine dams in the Three Sisters and Mount Jefferson wilderness areas, Oregon, United States Geological Survey Professional Paper, 1606, 11–40, https://doi.org/10.1007/BF01211117, 2001.

Osti, R. and Egashira, S.: Hydrodynamic characteristics of the Tam Pokhari glacial lake outburst flood in the Mt. Everest region, Nepal, Hydrol. Process., 23, 2943–2955, https://doi.org/10.1002/hyp.7405, 2009.

Prakash, C. and Nagarajan, R.: Outburst susceptibility assessment of moraine-dammed lakes in Western Himalaya using an analytic hierarchy process, Earth. Surf. Proc. Land., 42, 2306–2321, https://doi.org/10.1002/esp.4185, 2017.

Pudasaini, S. P.: A general two-phase debris flow model, J. Geo-phys. Res., 117, F03010, https://doi.org/10.1029/2011JF002186, 2012.

Pudasaini, S. P. and Mergili, M.: A multi-phase mass flow model, J. Geophys. Res-sol Ea, 124, 2920–2942, https://doi.org/10.1029/2019jf005204, 2019.

Qi, M. M., Liu, S. Y., Yao, X. J., Grünwald, R., and Liu, J.: Lake inventory and potentially dangerous glacial lakes in the Nyang Qu Basin of China between 1970 and 2016, J. Mt. Sci-Engl, 17, 851–870, https://doi.org/10.1007/s11629-019-5675-5, 2020.

Qin D. H., Dong, W. J., and Luo, Y.: Climate and environment change in China, China Meteorological Press, Beijing, 116-121, 2012.

Richardson, S. D. and Reynolds, J. M.: An overview of glacial hazards in the Himalayas, Quatern. Int., 65, 31–47, https://doi.org/10.1016/S1040-6182(99)00035-X, 2000.

Risio, M., Girolamo, P. D., and Beltrami, G. M.: Forecasting landslide generated Tsunamis: a review, the Tsunami threat-research and technology, 81–106, https://doi.org/10.5772/13767, 2011.

Rounce, D. R., McKinney, D. C., Lala, J. M., Byers, A. C., and Watson, C. S.: A new remote hazard and risk assessment framework for glacial lakes in the Nepal Himalaya, Hydrol. Earth Syst. Sci., 20, 3455–3475, https://doi.org/10.5194/hess-20-3455-2016, 2016.

Sakai, A., Yamada, T., and Fujita, K.: Volume change of Imja Glacial Lake in the Nepal Himalayas, International Symposium on Disaster Mitigation & Basin Wide Water Management, Niigata, 556–561. 2003.

Sakai, A.: Glacial lakes in the Himalayas: a review on formation and expansion processes, Global Environmental Research, 16, 23–30, 2012.

Sattar, A., Goswami, A., and Kulkarni, A. V.: Hydrodynamic moraine-breach modeling and outburst flood routing - a hazard assessment of the South Lhonak lake, Sikkim, Sci. Total. Environ., 668, 362–378, https://doi.org/10.1016/j.scitotenv.2019.02.388, 2019.

Sattar, A., Haritashya, U. K., Kargel, J. S., Leonard, G. J., and Chase, D. V.: Modeling lake outburst and downstream hazard assessment of the Lower Barun Glacial Lake, Nepal Himalaya, J. Hydrol., 598, 126208, https://doi.org/10.1016/j.jhydrol.2021.126208, 2021.

Schneider, D., Bartelt, P., Caplan-Auerbach, J., Christen, M., Huggel, C., and W. McArdell, B.: Insights into rock-ice avalanche dynamics by combined analysis of seismic recordings and a numerical avalanche model, J. Geophys. Res., 115, F04026, https://doi.org/10.1029/2010JF001734, 2010.

Schneider, D., Huggel, C., Cochachin, A., Guillén, S., and García, J.: Mapping hazards from glacier lake outburst floods based on modelling of process cascades at Lake 513, Carhuaz, Peru, Adv. Geosci, 35, 145–155, https://doi.org/10.5194/adgeo-35-145-2014, 2014.

Sharma, R. K., Pradhan, P., Sharma, N. P., and Shrestha, D. G.: Remote sensing and in situ-based assessment of rapidly growing South Lhonak glacial lake in eastern Himalaya, India, Nat. Hazards., 93, 393, https://doi.org/10.1007/s11069-018-

3348-2, 2018.

Shi, W. L., Yang, C. T., You, G. X., and Jin, M. X.: The measurement of reserve of glacier block lake on the upper stream of Yerqiang river and the calculation of its maximum flood, Arid Land Geography., 14, 31–35, 1991.

Shugar, D., Burr, A., Haritashya, U. K., Kargel, J. S., Watson, C. S., Kennedy, M. C., Bevington, A. R., Betts, R. A., Harrison, S., and Strattman, K.: Rapid worldwide growth of glacial lakes since 1990, Nat. Clim. Change., 10, 939–945, https://doi.org/10.1038/s41558-020-0855-4, 2020.

Song, C. Q., Sheng, Y. W., Ke, L. H., Nie, Y., and Wang, J. D.: Glacial lake evolution in the southeastern Tibetan Plateau and the cause of rapid expansion of proglacial lakes linked to glacial-hydrogeomorphic processes, J. Hydrol., 540, 504–514, https://doi.org/10.1016/j.jhydrol.2016.06.054, 2016.

Somos-Valenzuela, M. A., Chisolm, R. E., Rivas, D. S., Portocarrero, C., and McKinney, D. C.: Modeling glacial lake outburst flood process chain: the case of Lake Palcacocha and Huaraz, Peru, Hydrol. Earth Syst. Sci., 20, 2519–2543, https://doi.org/ 10.5194/hess-2015-512, 2016.

Specht, M., Specht, C., Lasota, H., and Cywiński, P.: Assessment of the steering precision of a hydrographic unmanned surface vessel (USV) along sounding profiles using a low-cost multi-global navigation satellite system (GNSS) receiver supported autopilot, Sensors-Basel, 19, 3939, https://doi.org/10.3390/s19183939, 2019.

Sun, M. P., Liu, S. Y., Yao, X. J., and Li, L.: The cause and potential hazard of glacial lake outburst flood occurred on July 5, 2013 in Jiali County, Tibet, Journal of Glaciology and Geocryology, 36, 158–165, https://doi.org/158-165,10.7522/j.issn.1000-0240.2014.0020, 2014.

Thompson, S., Benn, D. I., Mertes, J., and Luckman, A.: Stagnation and mass loss on a Himalayan debris-covered glacier: Processes, patterns and rates, J. Glaciol., 62, 467–485, https://doi.org/10.1017/jog.2016.37, 2016.

Veh, G., Korup, O., Specht, S. V., Roessner, S., and Walz, A.: Unchanged frequency of moraine-dammed glacial lake outburst floods in the Himalaya, Nat. Clim. Change., 9, 379–383, https://doi.org/10.1038/s41558-019-0437-5, 2019.

Vetsch, D., Siviglia, A., Bürgler, M., Caponi, F., Ehrbar, D., Facchini, M., Faeh, R., Farshi, D., Gerber, M., Gerke, E., Kammerer, S., Koch, A., Mueller, R., Peter, S., Rousselot, P., Vanzo, D., Veprek, R., Volz, C., Vonwiller, L., and Weberndorfer, M.: System manuals of BASEMENT, Version 2.8.2 Laboratory of Hydraulics, Glaciology and Hydrology (VAW). ETH Zurich. Available from http://www.basement.ethz.ch. [3 October 2022].

Vilímek, V., Emmer, A., Huggel, C., Schaub, Y., and Würmli, S.: Database of glacial lake outburst floods (GLOFs)-IPL project no. 179, Landslides, 11, 161–165, https://doi.org/10.1007/s10346-013-0448-7, 2013.

Wang, S. J., Che, Y. J., and Ma, X. G.: Integrated risk assessment of glacier lake outburst flood (GLOF) disaster over the Qinghai-Tibetan Plateau (QTP), Landslides, 17, 2849–2863, https://doi.org/10.1007/s10346-020-01443-1, 2020b.

Wang, S. J., Yang, Y., Gong, W., Che, Y., Ma, X., and Xie, J.: Reason analysis of the Jiwenco glacial lake outburst flood (GLOF) and potential hazard on the Qinghai-Tibetan Plateau, Remote Sens-Basel, 13, 3114, https://doi.org/10.3390/rs13163114, 2021.

Wang, W. C., Yao, T. D., Gao, Y., Yang, X. X., and Kattel, D. B.: A first-order method to identify potentially dangerous glacial lakes in a region of the southeastern Tibetan Plateau, Mt. Res. Dev., 31, 122–130, https://doi.org/10.1659/MRD-JOURNAL-D-10-00059.1, 2011a.

Wang, W. C., Yang, X. X., and Yao, T. D.: Evaluation of ASTER GDEM and SRTM and their suitability in hydraulic modelling of a glacial lake outburst flood in southeast Tibet, Hydrol. Process., 26, 213–225, https://doi.org/10.1002/hyp.8127, 2011b.

Wang, W. C., Yao, T. D., Yang, W., Joswiak, D., and Zhu, M. L.: Methods for assessing regional glacial lake variation and hazard in the southeastern Tibetan Plateau: a case study from the Boshula mountain range, China, Environ. Earth. Sci., 67, 1441–1450, https://doi.org/ 10.1007/s12665-012-1589-z, 2012.

Wang, W. C., Gao, Y., Anacona, P. I., Lei, Y. B., Xiang, Y., Zhang G. Q., Li, S. H., and Lu, A. X.: Integrated hazard

assessment of Cirenmaco glacial lake in Zhangzangbo valley, Central Himalayas, Geomorphology, 306, 292–305, https://doi.org/10.1016/j.geomorph.2015.08.013, 2015.

Wang, X., Liu, S. Y., Ding, Y. J., Guo, W. Q., Jiang, Z. L., Lin, J., and Han, Y.: An approach for estimating the breach probabilities of moraine-dammed lakes in the Chinese Himalayas using remote-sensing data, Nat. Hazards Earth Syst. Sci., 12, 3109–3122, https://doi.org/10.5194/nhess-12-3109-2012, 2012a.

Wang, X., Liu, S. Y., Guo, W. Q., Yao, X. J., Jiang, Z. L., and Han, Y. S.: Using remote sensing data to quantify changes in glacial lakes in the Chinese Himalaya, Mt. Res. Dev., 32, 203–212, https://doi.org/10.1659/MRD-JOURNAL-D-11-00044.1, 2012b.

Wang, X.: Methodology and application of moraine lake outburst hazard evaluation in the Chinese Himalayas, Science Press, Beijing, 2016.

Wang, X., Chai, K. G., Liu, S. Y., Wei, J. F., Jiang, Z. L., and Liu, Q. H.: Changes of glaciers and glacial lakes implying corridor-barrier effects and climate change in the Hengduan Shan, southeastern Tibetan Plateau, J. Glaciology., 63, 535–542, https://doi.org/10.1017/jog.2017.14, 2017.

Watanbe, T. and Rothacher, D.: The 1994 Lugge Tsho glacial lake outburst flood, Bhutan Himalaya, Mt. Res. Dev., 16, 77–81, https://doi.org/10.2307/3673897, 1996.

Watson, C. S., Quincey, D. J., Carrivick, J. L., Smith, M. W., Rowan, A. V., and Richardson, R.: Heterogeneous water storage and thermal regime of supraglacial ponds on debris covered glaciers, Earth. Surf. Proc. Land., 43, 229–241, https://doi.org/10.1002/esp.4236, 2018.

Westoby, M. J., Glasser, N. F., Brasington, J., Hambrey, M. J., Quincey, D. J., and Reynolds, J. M.: Modelling outburst floods from moraine-dammed glacial lakes, Earth-Sci. Rev., 134, 137–159, https://doi.org/10.1016/j.earscirev.2014.03.0092014, 2014.

Worni, R., Huggel, C., and Stoffel, M.: Glacial lakes in the Indian Himalayas - from an area-wide glacial lake inventory to an on-site and modeling based risk assessment of critical glacial lakes, Sci. Total Environ, 468, S71–S84, https://doi.org/10.1016/j.scitotenv.2012.11.043, 2013.

Worni, R., Huggel, C., Clague, J. J., Schaub, Y., and Stoffel, M.: Coupling glacial lake impact, dam breach, and flood processes: A modeling perspective, Geomorphology, 224, 161–176, https://doi.org/10.1016/j.geomorph.2014.06.031, 2014.

Wong, M. and Parker, G.: Reanalysis and correction of bed-load relation of meyer-peter and mã¼ller using their own database, Journal of Hydraulic Engineering, 132, 1159–1168, https://doi.org/10.1111/j.1600-0587.1978.tb00950.x, 2006.

Yan, R. J., Pang, S., Sun, H. B., and Pang, Y. J.: Development and missions of unmanned surface vehicle, J. Mar. Sci. Appl., 9, 451–457, https://doi.org/10.1007/s11804-010-1033-2, 2010.

Yang, W., Yao, T. D., Xu, B. Q., Wu, G. J., Ma, L. L., and Xin, X. D.: Quick ice mass loss and abrupt retreat of the maritime glaciers in the Kangri Karpo Mountains, southeast Tibetan Plateau, Chin, Sci. Bull., 53, 2547–2551, https://doi.org/10.1007/s11434-008-0288-3, 2008.

Yamada, T.: Glacier lake and its outburst flood in the Nepal Himalaya, Data Center for Glacier Research, Japanese Society of Snow and Ice, 1, 96, 1998.

Yamada, T., Naito, N., Kohshima, S., Fushimi, H., Nakazawa, F., Segawa, T., Uetake, J., Suzuki, R., Sato, N., Karma, Chhetri, I. K., Gyenden, L., Yabuki, H., and Chikita, K.: Outline of 2002: research activity on glaciers and glacier lakes in Lunana region, Bhutan Himalayas, Bull. Glaciol. Res., 21: 79–90, 2004.

Yao, X. J., Liu, S. Y., Sun, M. P., Wei, J. F., and Guo, W. Q.: Volume calculation and analysis of the changes in moraine-dammed lakes in the north Himalaya: a case study of Longbasaba lake, J. Glaciol, 58, 753–760, https://doi.org/10.3189/2012JoG11J048, 2012.

Yao, X. J., Liu, S. Y., Sun, M. P., and Zhang, X. J.: Study on the glacial lake outburst flood events in Tibet since the 20th century, Journal of Natural Resources, 8, 1377–1390, https://doi.org/10.11849/zrzyxb.2014.08.010, 2014.

Yuan, G. and Zeng, Q.: Glacier-dammed Lake in Southeastern Tibetan Plateau during the Last Glacial Maximum, J. Geol. Soc. India., 79, 295–301, https://doi.org/10.1007/s12594-012-0041-z, 2012.

Zemp, M., Huss, M., Thibert, E., Eckert, N., McNabb, R., Huber, J., Barandun, M., Machguth, H., Nussbaumer, S. U., Gartner-Roer, I., Thomson, L., Paul, F., Maussion, F., Kutuzov, S., and Cogley, J. G.: Global glacier mass changes and their contributions to sea-level rise from 1961 to 2016, Nature, 568, 382–386, https://doi.org/10.1038/s41586-019-1071-0, 2019.

Zhang, B., Liu, G. X., Zhang, R., Fu, Y., and Li, Z. L.: Monitoring dynamic evolution of the glacial lakes by using time series of Sentinel-1A SAR images, Remote Sens-Basel, 13, 1313, https://doi.org/10.3390/rs13071313, 2021.

Zhang, M. M., Chen, F., Tian, B. S., Liang, D., and Yang, A. Q.: High-frequency glacial lake mapping using time series of Sentinel-1A/1B SAR imagery: An assessment for southeastern Tibetan Plateau, Nat. Hazard. Earth. Sys., 1–18, https://doi.org/10.5194/nhess-2019-219, 2020.

Zhang, Y., Yao, X. J., Duan, H. Y., and Wang, Q.: Simulation of glacial lake outburst flood in Southeastern Qinghai-Tibet plateau - a case study of Jiwen Co Glacial Lake, Frontiers in Earth Science, 10: 1–13. https://doi: 10.3389/feart.2022.819526, 2022.

Zhang, D. H., Zhou, G., Li, W., Han, L., Zhang, S., Yao, X. J., and Duan, H. Y.: A robust glacial lake outburst hazard assessment system validated by GLOF event in 2020 in the Nidu Zangbo Basin, Tibetan Plateau, Catena, 220, 106734, https://doi.org/10.2139/ssrn.3962879, 2023.

Zheng, G. X., Mergili, M., Emmer, A., Allen, S., and Stoffel, M.: The 2020 glacial lake outburst flood at Jinwu Co, Tibet: causes, impacts, and implications for hazard and risk assessment, The Cryosphere, 15, 3159–3180, https://doi.org/10.5194/tc-2020-379, 2021.

Zhou, G. G. D., Zhou, M. J., Shrestha, M. S., Song, D. R., Choi, C. E., Cui, K. F. E., Peng, M., Shi, Z. M., Zhu, X. H., and Chen, H. Y.: Experimental investigation on the longitudinal evolution of land- slide dam breaching and outburst floods, Geomorphology 334, 29–43, https://doi.org/10.1016/j.geomorph.2019.02.035, 2019.

Zhou, L. X., Liu, J. K., and Li, Y. L.: Calculation method of mathematical model of the moraine dammed lake storage capacity, Science Technology and Engineering, 20, 9804–9809, 2020.